Cytometry Part A 69A:712–734 (2006)

Reviews

Imaging Spectrometer Fundamentals for Researchers in the Biosciences—A Tutorial

Jeremy M. Lerner*
LightForm Incorporated, Hillsborough, New Jersey

Received 30 August 2005; Revision Received 19 December 2005; Accepted 20 December 2005

Over the last 2 years there has been a dramatic increase in the number of bioscience laboratories using wavelength dispersive spectroscopy to study in vivo, in situ fluorescence. Transforming spectral information into an image provides a graphic means of mapping localized ionic, molecular, and protein–protein interactions. Spectroscopy also enables fluorophores with overlapping spectral features to be delineation. In this study, we provide the tools that a researcher needs to put into perspective instrumental contributions to a reported spectrum in order to gain greater understanding of the natural emission of the sample. We also show how to deduce the basic capabilities of a spectral confocal system. Finally, we show how to determine the true spectral bandwidth of an object, the illuminated area of a laser-excited object, and what is needed to optimize light throughput. © 2006 International Society for Analytical Cytology

Key terms: spectral imaging; spectrometer; spectrograph; PARISS; hyperspectral imaging; confocal; spectrometer design; wavelength calibration; spectral calibration

The use of spectroscopy has greatly simplified the task of characterizing and delineating autofluorescence, natural fluorophores, and multiple man-made fluorophores, many with overlapping spectral profiles, in the same sample. Consequently, spectroscopy is one of the fastest growing techniques to be found in a bioscience laboratory (1,2). It is also one of the least understood, especially when both spectral and spatial information is required. In this study, we focus on wavelength dispersive devices rather than those that acquire spectra sequentially by changing bandpass filters. The transformation of wavelength information into an image is often called hyperspectral or multispectral imaging, but these terms are so blurred that, given the current state of technology, using the simple term "spectral imaging" is appropriate.

This study provides the researcher with the tools to understand how spectrometers work, and how the limits of instrument performance can affect the accuracy, quality, validity, and interchangeability of acquired data. Spectrometers operate with multiple variables that have a significant influence on bandpass, wavelength dispersion, aberrations, and light throughput. To complicate matters further not all spectrometers work well with linear arrays or charge coupled devices (CCD) as a wavelength detectors. We try to put all these factors into perspective.

To provide background we also describe how readily available commercial, plane grating, concave holographic grating, and advanced prism-based spectrometers work, and discuss their inherent limitations and advantages.

The goal is to help a researcher optimize light throughput, check accuracy, and understand the real consequences of changing aperture sizes (such as a pinhole in a confocal system) on spectroscopic performance. When comparing spectroscopic results with those of others, it is important to understand that in some spectrometers spectral resolution degrades with an increase in the ratio of magnification to numerical aperture (NA), pinhole (or slit) size, and in other instruments spectral resolution is a constant. We also illustrate how to determine the undisclosed operating parameters of a commercial spectral confocal microscope.

There is a routine debate concerning the actual illuminated area of a sample in a laser confocal system. To help put this issue into perspective there is a section on light throughput as a function of variously scattering, laser-excited samples.

*Correspondence to: Jeremy M. Lerner, LightForm Inc., 601 Route 206, Suite 26-479, Hillsborough, NJ 08844, USA.
E-mail: jlerner@lightforminc.com
Published online in Wiley InterScience (www.interscience.wiley.com).
DOI: 10.1002/cyto.a.20242

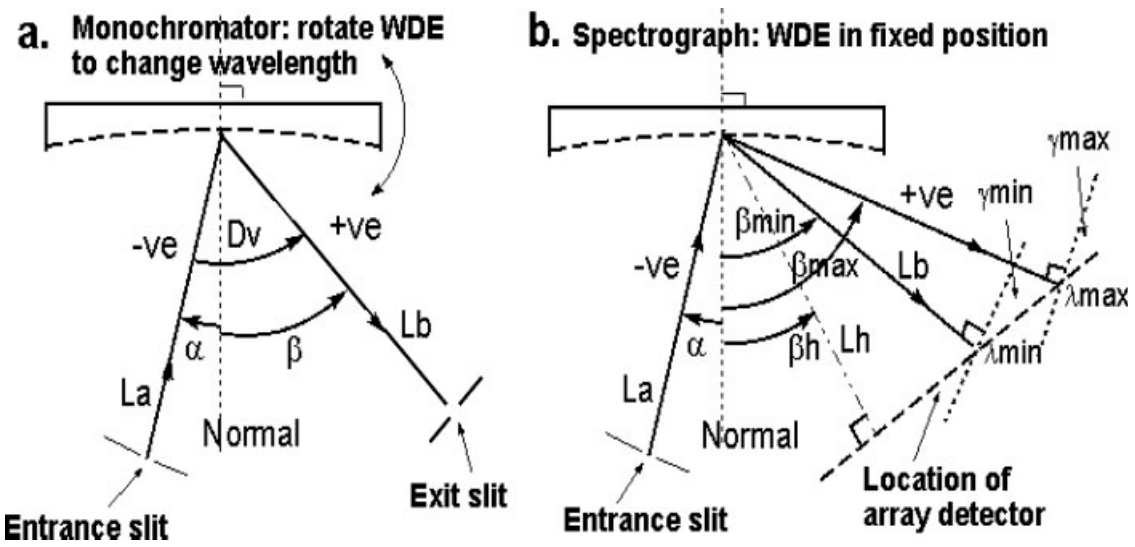

FIG. 1. Generic optical layout for both diffraction grating and prism spectrometers. (**a**) A monochromator with entrance and exit apertures in fixed locations where the WDE rotates to change wavelength; and (**b**) a spectrograph with a fixed WDE where the angle of diffraction (or refraction) varies with wavelength. A multielement detector located at the focal detects all wavelengths simultaneously, where α, angle of incidence; β, angle of diffraction (or refraction for a prism); *k*, order (prisms only refract in one order compared to diffraction gratings that present light in multiple orders); β_{min}, angle of diffraction, or refraction, at the shortest wavelength on an array; β_{max}, angle of diffraction, or refraction, at the longest wavelength on an array; λ, wavelength; Dv, fixed angle at the center of the WDE; Normal: a reference line perpendicular to the optic. Angles are measured from the normal; La, distance from the entrance aperture to the first active optic such as a collimating mirror; Lb, distance from the final active optic to the exit aperture or detector; Lh, Perpendicular distance from the final focusing optic to the focal plane in a "field-flattened" spectrograph; βh, angle measured from the normal to the grating to Lh; γ, inclination of a ray Lb, at a specific wavelength, to the focal plane in a "flat-field" spectrograph. An alternative approach in a spectrograph configuration is to translate an aperture/detector across the focal field.

WAVELENGTH DISPERSION THROUGH DIFFRACTION GRATINGS AND PRISMS

Regardless of the nature of its wavelength dispersive element (WDE), all spectrometers operate as a function of the same geometric optics. Light strikes the WDE at an angle of incidence, and depending on whether the WDE is a diffraction grating or prism, it is either diffracted or refracted at an angle of diffraction (refraction) that varies with wavelength. By the very nature of imaging spectroscopy, multiple wavelengths will be acquired to characterize an object. In a monochromator such as that shown in Figure 1a each wavelength is acquired sequentially and a photomultiplier tube (PMT) measures the signal at each wavelength (3–6).

In a spectrograph such as that shown in Figure 1b either a one-dimensional linear array of detector elements, or a matrix array such as a CCD acquire a series of wavelengths simultaneously. The spectrometer has to be designed to distribute the wavelength range of choice over the fixed dimensions of the detector. In other words, first the detector has to be chosen, and then the optics of the spectrometer has to be designed around it.

Although the same geometrical optic considerations apply to both prism and diffraction grating based spectrometers, in this study we illustrate the concepts using the diffraction grating equations. Most WDE-based systems require collimating and/or focusing optics to bring light from the entrance aperture and focus wavelength dispersed light onto the detector. For simplicity, collimating and focusing optics are not shown in Figure 1.

The theory behind diffraction gratings and prisms is well covered in the literature; so this section simply highlights the main issues that are of importance to the bioscientist (3,5–7).

"Need to Know" Diffraction Grating Equations

Diffraction gratings are available in three types: classically ruled (CR), holographic surface relief (HSRG), and volume holographic (VHG). CR and HSRG gratings work in reflection on flat (plano), concave, or convex surfaces. A VHG is typically used in transmission.

A classical diffraction grating is generated by mechanically "ruling" (actually burnishing) grooves into a coating of aluminum or gold on a glass blank. The first example of a ruled grating occurred in 1817 when Fraunhofer constructed an engine to rule diffraction gratings. Since then, advanced ruling engines have been developed, which have dramatically improved precision, accuracy, groove shape, spacing, and made it possible to rule very large, high-groove-density (up to 5,000 g/mm) gratings, even on curved surfaces.

Holographic gratings are recorded at the intersection of two expanded laser beams to form a series of periodic fringes in photoresist, which, after processing, form sinusoidal grooves. A major breakthrough occurred in 1969 when Labeyrie, Cordelle, Flamand, and Pieuchard at Jobin Yvon in France introduced concave aberration-corrected holographic gratings (ACHG) that greatly reduced or eliminated astigmatism and field curvature. A key advantage to these gratings is that they do not require any additional fo-

cusing or collimating optics. This simplicity makes them very attractive for use as the WDE in compact monochromators or spectrographs. Examples of the use of ACHG gratings are described later in this paper (3,6,8–10).

The diffraction grating equation applies to both ruled and holographic gratings:

$$\sin\alpha + \sin\beta = kn\lambda \qquad (1)$$

where the terms are based on those shown in the legend of Figure 1.

The angles of incidence and diffraction, or refraction, both vary as a function of wavelength in a monochromator, but the angle of incidence is fixed in a spectrograph, and the angles of diffraction vary with wavelength (Fig. 1).

Transmission gratings modify Eq. (1) to accommodate its refractive index and the thickness of its glass substrate.

The Deviation angle (Dv) is the fixed angle that forms the center of the entrance slit, the center of the WDE, and the center of the exit slit and is given by:

$$\mathrm{Dv} = \beta - \alpha \qquad (2)$$

In a spectrograph where the location of an array detector is fixed, there will be a different value of Dv for the rays striking the first pixel on the array when compared with that for rays striking the last pixel on the array, corresponding to λ_{max} and λ_{min}.

The value of Dv is a constant of the system and does not change if the groove density of the diffraction grating is changed. However, the wavelengths appearing at λ_{max} and λ_{min} will change according to Eq. (1). To vary the spectral range on the array, the WDE will be rotated.

Angular Dispersion

The angular spread between two wavelengths is given by:

$$\frac{d\beta}{d\lambda} = \frac{kn * 10^{-6}}{\cos\beta} \qquad \text{(radians)}$$

where n, groove density; k, order; $d\beta$, the angle in radians; $d\lambda$, the separation between two wavelengths in nanometers (nm).

Linear Dispersion

Linear dispersion is measured in nanometers per millimeter (nm/mm) and defines the extent to which a spectral interval is physically spread out across a focal field in millimeters. A lower dispersion value increases the distance between wavelengths and the potential for higher spectral resolution. Linear dispersion is wavelength-specific and is measured perpendicular to the exit ray Lb at the wavelength of interest.

$$\frac{d\lambda}{dx} = \frac{10^6 \cos\beta}{(kn\mathrm{Lb})} \qquad (3)$$

Dispersion in a spectrograph varies with the length of Lb as a function of wavelength and also by the inclination of Lb to the detector plane at the focal field γ such that:

$$\frac{d\lambda}{dx} = \frac{10^6 \cos\beta * \cos\gamma}{(kn\mathrm{Lb})}$$

In summary, linear dispersion varies with wavelength as a function of the angle of diffraction (β), the distance Lb at each wavelength, and the inclination (γ) of Lb to the focal field.

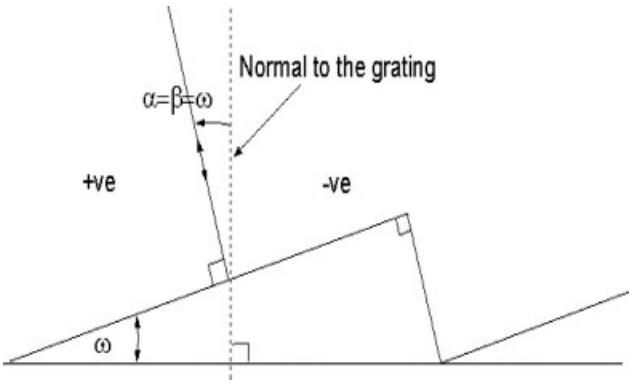

FIG. 2. A classically ruled blazed diffraction grating. This figure illustrates the Littrow configuration, where ω = the "Blaze" angle and $\omega = a = b$. It is rare for this geometry to be used in practice, but catalog specifications for efficiency and blaze are always quoted in Littrow.

Blazing or Wavelength Optimized Diffraction Gratings

Ruled diffraction gratings are optimized for maximum efficiency at only one wavelength known as the "blaze" wavelength. Classically ruled gratings have a triangular shape with a blaze angle that is chosen to produce maximum diffraction efficiency at a particular wavelength in a Littrow configuration (when the angle of incidence equals the angle of diffraction, as shown in Figure 2.

The diffraction grating Eq. (1) in Littrow simplifies to:

$$2\sin(\omega) = kn\lambda \qquad (4)$$

where $\omega = \alpha = \beta$.

Catalogs typically specify diffraction gratings in terms of groove density (n), blaze wavelength, and blaze angle. A Littrow geometry is not commonly used, and in a spectrograph is impossible, except at a single wavelength; however, deviations from Littrow rarely make a big difference to an efficiency profile when deviation angles are less than 40°. The use of the term "diffraction efficiency" always means the reflectivity relative to the metal coating the grating at the wavelength in question. For example, if a grating is coated with gold or aluminum, and is 50% reflective at a particular wavelength, then a diffraction grating quoted with 50% diffraction efficiency will diffract 25% of the incident light at that wavelength. The remainder will appear in other orders including the zero order (a reflection off the grating as if it were a mirror. See the following section for detailed discussion on diffraction grating orders.)

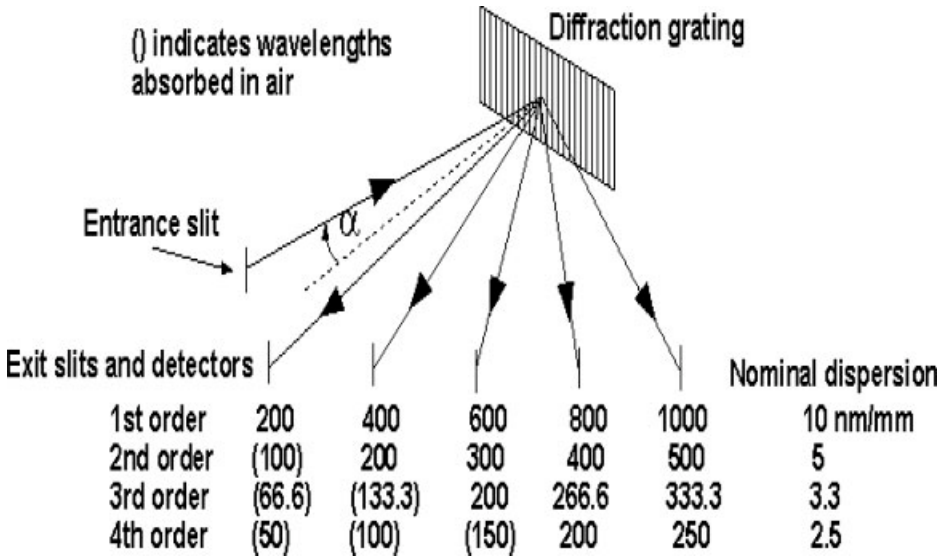

FIG. 3. Virtually all diffraction gratings diffract light into "orders," with the "first" order used to present spectral data. However, all shorter wavelength multiples of first order wavelengths will commingle with the first order spectrum. For example, 400, 266.6, and 200 nm will be superimposed on 800 nm in first order; if they are present in the light source. This can be a significant spectral contamination problem when the quantum efficiency of the detector is greater at shorter wavelengths than longer wavelengths.

A good rule of thumb is to assume that relative diffraction efficiency will drop by 50% at 0.67 times the blaze wavelength and at 1.8 times the blaze wavelength. For example, if the grating is blazed at 400 nm, the relative diffraction efficiency level is above 50% over the range of 267–720 nm.

Diffraction Grating Orders

A diffraction grating acts like a mirror when the angle of incidence (α) equals minus the angle of diffraction ($\alpha = -\beta$). This is known as the "zero"-order reflection. However, a diffraction grating can have an almost unlimited number of orders depending on the wavelength range and wavelengths present in the light source. Figure 3 shows a diffraction grating presenting 200–1,000 nm in first order ($k = 1$) in the focal field of a spectrograph. For given values of α, β, and groove density, the grating Eq. (1) simplifies to:

$$k\lambda = \text{constant}$$

From Eq. (4), we can see that a grating blazed when $k = 1$ is also blazed in all higher orders. For example, a grating blazed at 800 nm is also blazed at 400, 267, and 200 nm.

All wavelengths are diffracted simultaneously; so all orders, which can be present, will be present. Therefore, if 600 nm is diffracted into first order, then 300 nm will be present in second order, 200 nm in third order, and so on, and light from all orders will be commingled. Assuming that all wavelengths are present in the light source, the only way to prevent higher orders from contaminating first-order light is to use some form of blocking filter. If the wavelength range is from 200 to 399 nm, no order sorting filters are needed, because wavelengths below 200 nm are absorbed in the atmosphere. When wavelengths appear in multiple orders, this causes reduced diffraction efficiency in first order. Increasing the groove density and reducing the wavelength range reduces higher order possibilities, and increases overall first-order grating efficiency.

Linear dispersion also varies linearly with order; in fact, Echelle grating spectrometers take advantage of increased dispersion to increase spectral resolution by working only in high orders. A prism is used following the grating for "order sorting" up to 80 diffraction orders. The net result is that Echelle spectrometers deliver very high-spectral resolution (<0.1 nm, FWHM at 436 nm even though the groove density of the diffraction grating is only 52 g/mm), and can cover the wavelength range from 200 to 900 nm simultaneously (e.g., the "Mechelle," Andor Corp, Belfast, Northern Ireland).

Prisms work in a single order; therefore, their inherent efficiency profiles are significantly flatter and higher than those of gratings and, of course, do not need order-sorting filters. In addition, the wavelength transmission of most glasses is very high (>90%) over the majority of the visible and near infrared (up to about 1,000 nm).

Diffraction Gratings—Pros and Cons

Classically ruled reflection gratings. These can be very efficient at the blaze wavelength especially in Littrow. Ion lasers rely on this property to produce high-energy, high-efficiency emission at target wavelengths. Wavelength blazing can be achieved anywhere in the spectrum from the X-ray to the far infrared, and is typically polarization dependant. Master ruled gratings can be replicated with very high fidelity to make a very inexpensive optic.

On the downside, high-groove-density gratings can produce "ghosts" due to periodic ruling errors that vary as the square of the groove density (n) and order (k). Modern gratings have considerably reduced ghosting with the use of interferometrically controlled ruling engines. Plane diffraction gratings must be used in conjunction with collimating and focusing optics. Stray light (scatter) can be up to a factor of 10, greater than holographically produced gratings.

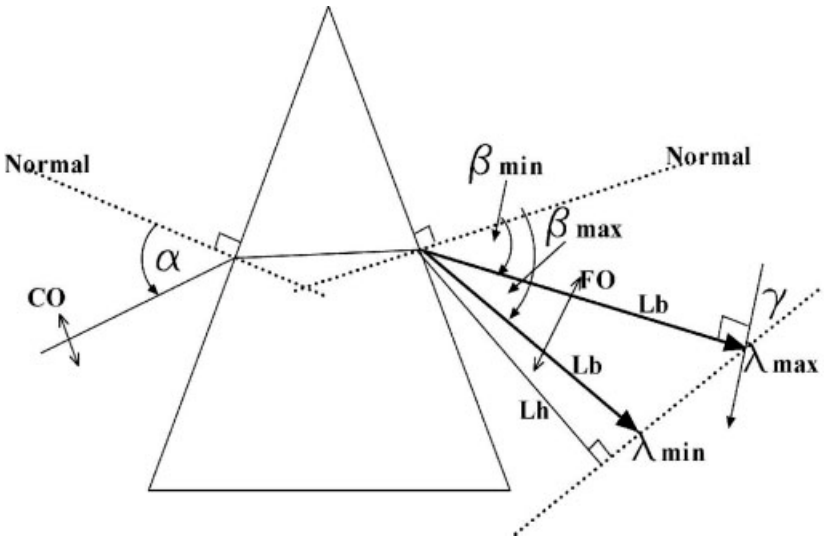

FIG. 4. A simplified schematic of refraction through a prism. Just as with diffraction gratings, there are angles of incidence and refraction (rather than diffraction), and a need to collimate light onto the prism and focus refracted wavelengths onto the wavelength dispersion plane.

Holographic surface relief diffraction gratings. HSRGs were developed in parallel, and essentially independently, by Labeyrie and Flamand in France, and Rudolph and Schmahl in Germany. HSRGs offer up to a full-order of magnitude less stray light than classically ruled gratings, absolutely no ghosts, and reduced polarization dependence. These advantages become significant at groove densities at or in excess of 600 g/mm, and/or for use below 400 nm.

Basic HSRGs tend to offer less diffraction efficiency than a classically ruled grating, because the groove profile is sinusoidal. This has since been mitigated by ion-etching triangular grooves to "blaze" the groove profile (11). HSRGs are typically inefficient at wavelengths much above 2 μm where low groove densities are necessary, in which case classically ruled gratings are superior.

Both classically ruled and holographic surface relief gratings are routinely replicated with very high fidelity and make a very inexpensive optic, especially considering the high level of technology and expertise that goes into making them.

Volume holographic gratings. The diffraction efficiency at blaze of a VHG can be high (>70%) over a particular wavelength range, but like plane reflection gratings, they need collimating and focusing optics when used as the WDE in a spectrometer. Mirrors make the best choice for collimating and focusing light because they are free of chromatic aberration; however, because a VHG usually works in transmission, there is a tendency for instrument designers to use lenses as collimators and focusers to provide an approximately in-line system.

The lens approach is not without problems due to reflections off lens edges, ghosting off lens surfaces, residual aberrations, including astigmatism at peripheral wavelengths, degraded diffracted wavefront, and a restricted wavelength range that can be limited by the degree of chromatic aberration correction over the operating wavelength range. For low-resolution systems, a VHG can be a good solution, but the cost of a VHG can be very high when compared with that of a replicated surface relief diffraction grating.

Wavelength Dispersion Through a Prism

Sir Isaac Newton first described the properties of a prism in 1670. Dr. Arnold Beckman produced the most successful UV spectrometer (arguably any spectrometer) ever built, the Beckman DU, by using a prism as the WDE. Indeed, Beckman Instruments owes much of its initial success to this instrument.

Figure 4 shows a simplified schematic of refraction through a prism (4,12,13). Essentially, the operating parameters (α,β,γ, Lb, Lh) are identical to those in a diffraction grating system. The same equations can be used to determine angular and linear dispersion, but cannot be used to calculate the values of the angles of incidence and refraction (α,β). Most classical prism spectrometers, like diffraction gratings, cannot be used without collimating and focusing optics, shown in Figure 4 as CO and FO.

The angle of refraction (β) varies with the refractive index of the prism material at each wavelength. For a flint glass prism, the linear wavelength dispersion at 436 nm is about four times greater than that at 611 nm, delivering approximately four times higher spectral resolution in the blue than in the red. Nonlinear wavelength dispersion makes it easy to "pack" an extended wavelength range onto a smaller detector array size. For example, the wavelength range from 400 to 800 nm can be accommodated by a ½-inch array chip when compared with a diffraction grating, which would require a 2/3-inch chip to provide the same spectral range and competitive spectral resolution.

Pros and Cons of Prisms

A prism offers a wide range of glass materials to ensure very high-transmission efficiency from 400 to 1,000 nm (>90%), good transmission efficiency down to 360 nm (~40%), and optimum refractive index characteristics over

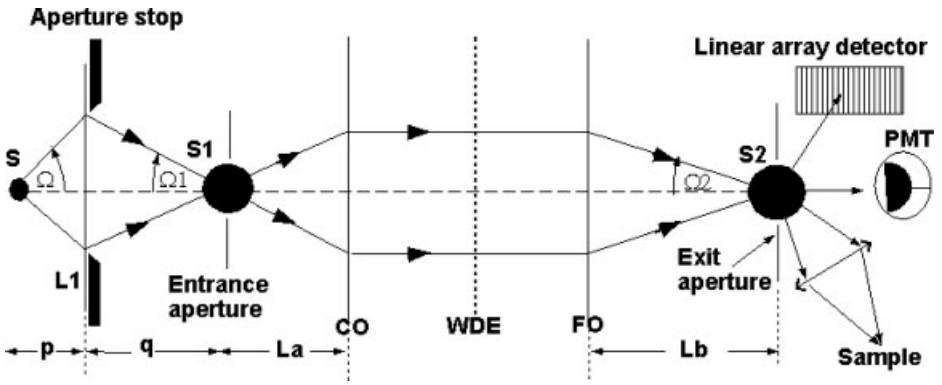

FIG. 5. Generalized format of a wavelength dispersive spectrometer. An object in the FOV with an area "*S*" is imaged onto the entrance aperture (slit or a pinhole) of a spectrometer with an area S_1. The aperture must accommodate the full size of the image of the object to prevent loss of light. Light is collimated onto the WDE and then focused onto the exit aperture. Light passing through the exit aperture can either be measured or used to excite or illuminate an object. All apertures must match the size of the image of "*S*," and all optics must accommodate the incident numerical aperture to prevent vignetting.

almost any wavelength range of choice. Light throughput is enhanced because wavelengths are only refracted into a single order. Scattered light characteristics are exceptionally good; exceeding most, if not all diffraction gratings.

It is relatively easy to exchange one diffraction grating with a particular groove density with another of different groove density, whereas this is impractical with a prism. In general, diffraction gratings provide significantly higher spectral resolution than prisms in monochromator mode. In spectrograph mode, it is the width of the entrance aperture and the length of the detector that determines bandpass and wavelength range; consequently, in this mode, the spectral resolution of prisms and diffraction gratings are competitive.

GEOMETRIC OPTICAL CONSIDERATIONS OF WAVELENGTH DISPERSIVE SPECTROMETERS

Wavelength Dispersive Spectrometer Designs

Image transfer basics. Wavelength dispersive spectrometers come in many optical configurations; however, they all follow a generalized format consistent with Figure 5. Regardless of the WDE in the spectrometer, light has to be collected from an object in the field of view (FOV). In an optimized system, optic L_1 can be the microscope objective or a telescope, and projects an image of an object with area, *S*, onto the entrance aperture of the spectrometer at a NA consistent with the NA of the optics of the spectrometer. To prevent vignetting, the entrance aperture must be matched in size to the image of the object with area, S_1.

As shown, an optic, CO, collimates light passing through the entrance aperture onto the WDE. The WDE diffracts or refracts collimated, wavelength-dispersed light that is focused by an optic, FO, onto an exit aperture or array detector. The exit aperture should be matched to the size of the wavelength dispersed image of the entrance aperture (S_2). A photomultiplier tube, linear array, or CCD can then measure photon flux at each wavelength. The geometry illustrated in Figure 5 also applies to an ACHG and other active optic configurations in which case CO and/or FO can be ignored. The basic principle, however, remains intact.

If the spectrometer is designed to operate as a monochromator, then each wavelength is selected sequentially by rotating the WDE, and an increment of the spectrum, with a given bandpass, passes through an exit aperture in a fixed location Figure 1a. After the aperture, the monochromatic light can either be used to illuminate or excite a sample or it can be passed to a measurement device, such as a PMT or diode. If the spectrometer is configured as a spectrograph, then an entire spectral range can be imaged simultaneously onto an array detector. In special cases, a spectrograph can be designed to correct severe aberrations, such as astigmatism, spherical aberration, coma, and correct field curvature, for use with a matrix array detector, such as a CCD. Aberration-corrected instruments of this type can be used for spectral topographical mapping to create images with considerable data content (4,5,14).

Aperture matching ensures lossless energy transfer. Figure 5 depicts an object in the FOV with an area *S* that is imaged onto an entrance aperture by an optic L_1. The areas of *S*, S_1, and S_2 will never be equal in a WDE-based spectrometer; consequently, a failure to match aperture sizes will either result in lost photons at the detector, or, if the apertures are too large, will suffer from increased stray light.

First let us consider the effects of magnification, or demagnification, on photon flux density taking the entrance optic L_1 as an example:

$$\begin{aligned}\text{Magnification} &= \text{SQRT}(S_1/S) = q/p = \sin\Omega_1/\sin\Omega \\ &= \text{NA}_{\text{in}}/\text{NA}_{\text{out}} = F\ \text{number}_{\text{out}}/F\ \text{number}_{\text{in}}\end{aligned} \tag{5}$$

The same relationships apply following the entrance slit through the spectrometer, where SQRT is the square root; *S* is the location and area of an object in the FOV; S_1, S_2 are the areas of projected images of *S*; *p* is the distance of the object with area *S* from optic L_1; *q* is the distance from L_1 to the entrance aperture; La is the distance from center of the entrance aperture to the center of the first active (often collimating) optic, or the center of a concave grating; Lb is the distance from the center of the focusing optic to the exit aperture or from the center of a concave

grating to the exit aperture; Ω is the half angle subtended by L_1; Ω_1 is the half angle subtended by focusing optic FO. NA_{in} is NA into L_1 (given by sin Ω); NA_{out} is NA leaving L_1 (given by sin Ω_1); and *F* number is *F#* = projected width of an optic/image distance (e.g., $F\#_{in}$ of L_1 = diameter/*p*; $F\#_{out} = L_1/q$).

$$\mathrm{NA} = \mu \sin \Omega \tag{6}$$

where μ is the angle of refraction. For most spectrometers, this is unity because spectrometers almost always operate in air.

$$F \text{ number } (F\#) = 1/(2\mathrm{NA}) \tag{7}$$

(Note: *F* number should be calculated from the NA not vice versa. This is due to the difficulty in identifying the position of the principle plane that defines the "effective diameter," or projected width, of a lens or mirror used in an off-axis configuration. When tan α (tan α = width WDE/Lb) is approximately equal to sin α, Eq. (7) is reversible; consequently, when NA >0.16, we can use Eq. (7) to convert *F* number to NA and back again. NA is an absolute value; *F* number is a relative value.)

As we progress through the remaining optics in the system, the image of *S* will undergo magnification and/or demagnification and photon density will be given by:

$$\begin{aligned}\text{Photon density} &= S_1/S = (q/p)^2 = (\mathrm{NA_{int}}/\mathrm{NA_{out}})^2 \\ &= (F\#_{out}/F\#_{in})^2\end{aligned} \tag{8}$$

The *F#* and NA relationships in Eq. (8) will be familiar to photographers and fluorescence imagers, because they directly govern relative exposure time at constant magnification.

Calculating Light Throughput

Nothing is more important than ensuring that all available light is transferred through the system. Geometric light throughput or Etendue defines the ability of an optical system to accept and transfer light. Etendue, also known as the "geometric extent," is a constant of an optical system and represents the "bottleneck" when considering the transfer of light. A failure to preserve the nominal value of the Etendue will result in a loss of real signal. Using Figure 5:

$$\begin{aligned}\text{Etendue} = G &= S(\sin\Omega)^2 = S_1(\sin\Omega_1)^2 \\ &= S_2(\sin\Omega_2)^2 = ...\end{aligned}$$

We can replace (sin Ω) with NA, and the Etendue equation simplifies to:

$$G = S^*(\mathrm{NA})^2 \tag{9}$$

The Etendue equation enables us to optimize the light throughput of any series of optics to ensure that the maximum available real signal is either passed to the detector or illuminates a sample. It tells us that the areas of apertures must be matched to collect all available light. It also tells us that the optics must accommodate the cone angles of light passing through the system.

In confocal microscopy, the Etendue equation can be used to test and determine how well a system is optimized, and the functional area of a laser-excited sample. We show an example of this later in the paper.

Real Life Bandpass and Resolution Characteristics of a Spectrometer

Theoretical resolution of a diffraction grating. The "resolving power," *R*, of a diffraction grating is at best an impractical, theoretical concept and is given by:

$$R = \lambda/d\lambda$$

where $d\lambda$ is the difference in wavelength between two spectral lines of equal intensity. Resolution is the ultimate ability of an instrument to separate two spectral lines. By the Raleigh criterion, two peaks are considered resolved when the maximum of one falls on the first minimum of the other. It can be shown that:

$$R = \lambda/d\lambda = knW_g = kN$$

where λ, the central wavelength to be resolved; W_g, the illuminated width of the grating; and *N*, the total number of grooves on the illuminated width of the grating.

Actual spectral resolution and bandpass depends on the width of the entrance aperture and the focal length of the system; so numerical resolution, *R*, should not be confused with observed resolution or bandpass of an instrument system. Hence, the original comment that resolving power is an impractical concept. It is only included for completeness.

Observed instrumental spectral resolution. Bandpass and resolution can be easily determined in any instrument by using a light source that emits a spectrum with a pure monochromatic line, λ_0. Figure 6a shows the natural "real" line width. Figure 6b shows how it would be characterized by a perfect spectrometer; so Figure 6b should be identical to Figure 6a.

Spectrometers are not perfect and record a line spectrum with finite width. This is known as the "instrumental line profile" and can be determined by characterizing the spectrum of a single mode laser or with a low-pressure Hg^+/Ar^+ emission lamp with the entrance and exit slits at minimum width. The bandpass is the full width at half maximum (FWHM) of the recorded spectrum Figure 6c.

In its simplest case, the bandpass of a spectral feature presented by the FOV is influenced by its natural line width, the influence of the slits, and the resolution of the instrument. For a monochromatic emission and a high-resolution spectrometer, the instrumental bandpass (BP) is given by:

$$\mathrm{BP_{sw}} = \mathrm{Disp} * W_{exap} \tag{10}$$

where Disp is the linear wavelength dispersion (in nm/mm) at a particular wavelength; W_{exap} is the width of the

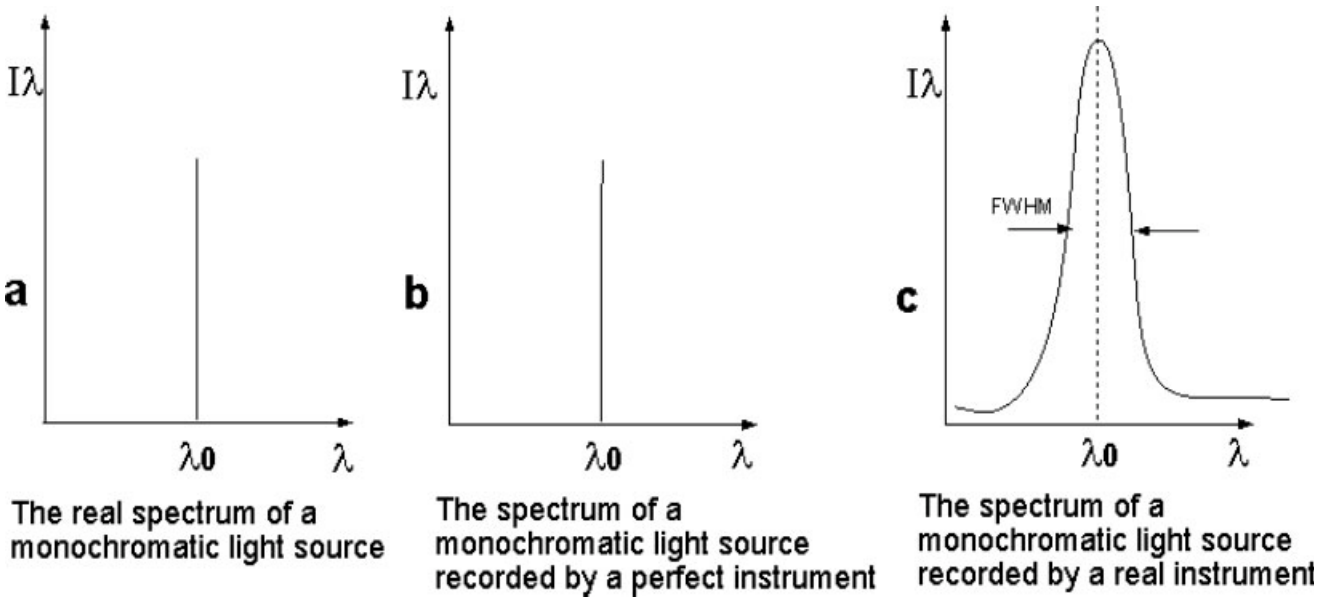

FIG. 6. The natural spectrum of a pure monochromatic light source (**a**); the same light source imaged through a theoretically "perfect" spectrometer (**b**); the pure monochromatic light imaged through a real-life spectrometer (**c**). The finite bandwidth (FWHM) is an instrumental function that is imposed on the natural bandwidth of the monochromatic light.

exit aperture or width of the image of the entrance aperture, whichever is greater.

The total recorded bandpass, BP_{net}, for an emission with finite spectral bandwidth, such as a fluorescence emission, assuming an approximately Gaussian distribution, is given by the "generalized bandpass equation" for a real emission:

$$BP_{net} = SQRT(BP_{nat}^2 + BP_{slit}^2 + BP_{res}^2) \qquad (11)$$

where BP_{net} is the net bandpass after accommodating the finite emission bandwidth of the light source and instrumental factors; SQRT is the square root; BP_{nat} is the natural spectral bandwidth of the emitting source; BP_{slit} is the bandpass determined by the bandpass Eq. (10); BP_{res} is the limiting resolution of the instrument (ultimate bandpass with a line emission source).

In real world acquisitions, the FWHM of a typical fluorescence emission is significantly greater than the limiting spectral resolution of the instrument; therefore, the reported resolution will be dominated by the bandpass determined by the slit width and the natural spectral bandwidth of the natural emission spectrum.

In essence, real life bandpass and resolution indicate the limits of a finite instrument's ability to separate real adjacent spectral features. Bandpass is set by the user, and resolution is limited by the functional limits of the instrument. The smallest possible bandpass is the resolution, and is determined when the FWHM of a monochromatic emission line is not reduced even when the slit width continues to be narrowed.

By rearranging Eq. (3), Disp = BP/W_{exap}; where W_{exap} is the FWHM of a monochromatic emission line, it is possible to calculate the linear dispersion of an instrument when the bandpass and distance one bandpass occupies are known. For example, if the light source is a monochromatic emission line from a low-pressure Hg lamp and the FWHM in Figure 6c is 1 nm, and occupies three 9 μm pixels on a CCD, then we know that the linear dispersion at 436 nm is 37 nm/mm (1/3*0.009) corresponding to BP_{net} in Eq. (11). Therefore, by knowing the functional operating characteristics of a spectrometer and rearranging Eq. (11), it is possible to reveal the natural spectral bandwidth of an emitting source.

If a light source emits a continuum, then the resolution is the smallest spectral increment that can be isolated, and the bandpass is a user selected spectral increment.

Magnification and System Anamorphism

We know from Eq. (10) that bandpass is determined by the product of linear dispersion, and either the image of the entrance aperture or the exit aperture, whichever is greater. However, the width of the image of the entrance slit aperture, shown as W^* in Figure 7, for either a monochromator or a spectrograph varies with wavelength.

Note that $W^* = W_{exap}$ when the width of the image of the entrance aperture is the same as the exit aperture. In a confocal system or a spectrometer with a fiber optic feed, the aperture could be a pinhole or a circle, rather than a slit.

The projected height can be determined by considering the magnification or demagnification through the system. Sometimes, it is more convenient to use *F* number, rather than NA. We can calculate the projected width of the entrance and exit slits by $W \cos \alpha$, and $W^* \cos \beta$ as perceived by the WDE, and divide these values by the entrance

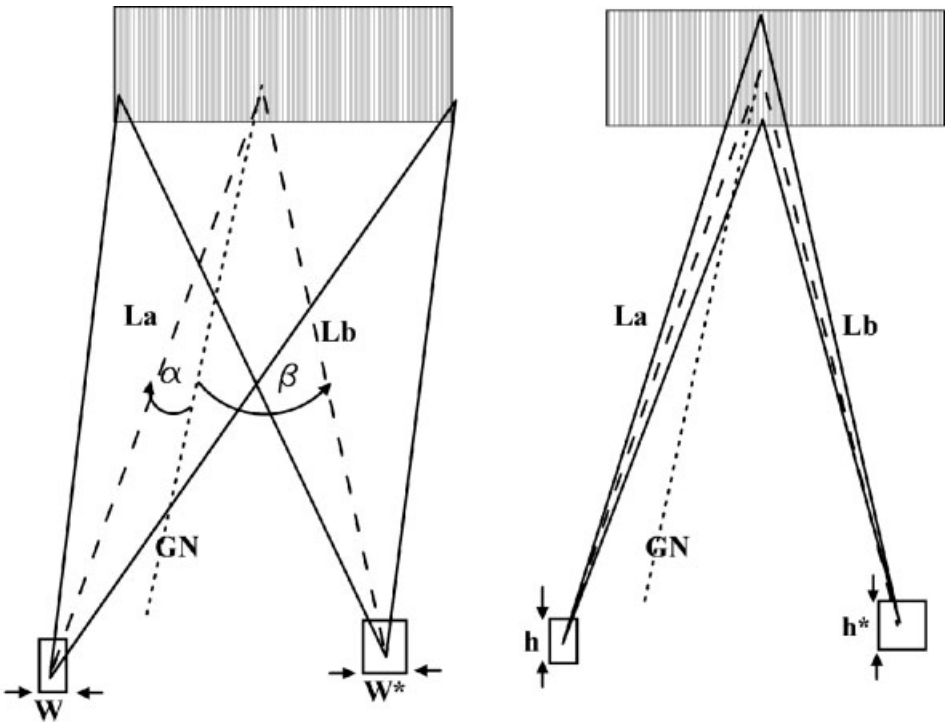

FIG. 7. System anamorphism results in an image of the entrance aperture appearing with a different width at each wavelength. The height of the slit is a constant in a monochromator, when Lb is fixed, ($b = b^*$) and a variable in a spectrograph when there is a different Lb for each wavelength ($b \neq b^*$).

and exit arm lengths to obtain the input and output *F* numbers.

$$F\#_{\text{out}} = \frac{W^* \cos\beta}{\text{Lb}}$$

$$F\#_{\text{in}} = \frac{W \cos\alpha}{\text{La}}$$

Therefore:

$$W^* = \frac{W \cos\alpha\, \text{Lb}}{\cos\beta\, \text{La}} \qquad (12)$$

We can now substitute Eqs. (3) and (12) into Eq. (10) to obtain the relationship:

$$\text{BP} = \frac{\text{W} \cos\alpha\, \text{Lb}\, 10^6 \cos\beta}{\cos\beta\, \text{La}\, kn\text{Lb}} \times (\text{projected slit width multiplied by linear dispersion})$$

$$\text{BP} = \frac{10^6 W \cos\alpha}{kn\text{La}} \qquad (13)$$

From Eqs. (13) and (3), we note that bandpass is a function of the angle of incidence, and linear dispersion a function of the angle of diffraction, or refraction.

Using Eq. (12), we can match the width of the exit slit to W^* or assign the correct number of detector elements in a linear or matrix array so as to maximize real signal throughput. This is of key importance for a diffraction grating system with a wide wavelength range and a long λ_{max}. The reverse is true for a prism-based system. With a diffraction grating, the angle of diffraction increases with wavelength; however, in a prism system, the angle of refraction varies inversely with wavelength. The height of the image of the entrance slit in the exit plane is determined by the ratio of the arm lengths alone:

$$b^* = \frac{b\, \text{Lb}}{\text{La}}$$

In the case of a spectrograph, the arm length Lb varies with wavelength; consequently, the vertical magnification also varies with wavelength. In a monochromator, the length Lb will be fixed unless the exit slit is translated across the spectrum to select wavelength, such as in a Leica SP series spectral confocal system.

How to Estimate the Operating Conditions of a Spectral Confocal Microscope

The equations listed in the previous sections are those that are needed to estimate the groove densities of diffraction gratings, focal length, changes in wavelength dispersion, theoretical bandpass, magnification of the pinhole, and the optical geometry (Dv angles). All we need to know in advance is the observed wavelength-range over a known width of an array detector.

Nikon C1-Si spectral imaging system with an IPMT linear array detector. Let us take as an example the Nikon C1-Si spectral imaging system. From published literature, we are informed that a user can sample a spectrum in 2.5, 5, or 10 nm increments, in what Nikon refers to "wavelength resolution," by exchanging three diffraction

Table 1
Estimated Geometric Parameters for a WSI of 2.5 nm

Observed (*F*) wavelength range (nm)	Eq. (1) (*C*) β (°)	Eq. (2) (*C*) Dv (°)	Eq. (12) (*C*) Pinhole (mm)	Eq. (3) (*C*) Disp (nm/mm)
531	11.04	−15.46	0.091	2.46
569	13.70	−12.80	0.092	2.44
607	16.39	−10.11	0.093	2.41

WSI = 2.5 nm; total length of the IMPT array detector = 32 mm; diffraction grating = 1,200 g/mm; angle of incidence α = 26.5°; focal length 332 mm; pinhole diameter = 100 mm. (*C*) = computed, (*F*) = actual observed values. The value of α was iterated; and Lb was calculated using the wavelength dispersion at the center of the chip of 2.44 nm/mm. This simple approach provides a good approximation.

gratings. It is more accurate to refer to these settings as the "wavelength sampling increment" (WSI). The use of three gratings implies that the wavelength dispersion will increase by a factor of two and four, based on the 10 nm condition. From Eq. (3), we know that to change dispersion we must either change the focal length (Lb) or the groove density (*n*). Consequently, we know that it is the groove density that will change because Lb is fixed. For this exercise, we took the pinhole to be 100 μm in diameter.

Observed wavelength scans acquired with a 2.5 nm WSI places the wavelength range of 531–607 nm across a 32 element, imaging photomultiplier tube (IPMT), linear array detector (Hamamatsu Corp, Bridgewater, NJ) in a single shot. The elements are on 1 mm centers with an active width of 800 μm, 7 mm in height, with 200 μm dead-space between elements, and each spectrum will be characterized by up to 32 wavelength data points (WDP).

(Note: As described the term "wavelength resolution" is really the WSI. The actual resolution, calculated by measuring the FWHM of a monochromatic emission line, will be between 2.5, 5, or 10 nm only when an image of the entrance pinhole strikes the center of an IPMT detector element.)

Therefore, the wavelength dispersion is 75.6 nm (607–531.4) spread over 31 mm (allowing 2 × 0.5 mm from center-to-center) for an average wavelength dispersion of 2.44 nm/mm (76/31). From diffraction grating catalogs, we note that off-the-shelf gratings are available in 150, 300, 600, 1,200, 1,800, and 2,400 g/mm, blazed at a variety of wavelengths. (Horiba/Jobin Yvon Edison NJ, Newport Corp-Richardson Gratings, Rochester NY).

The easiest way to estimate the geometric parameters is to construct Table 1 in an Excel spreadsheet. Then, select a catalog diffraction grating, vary α, and calculate the precise value of Lb using 2.44 nm/mm dispersion at the center of the chip at 569 nm (the wavelength that falls on the center detector element), using Eq. (3).

This process will display the Dv values at the extremes and the center of the wavelength range. The Dv values are then *fixed* and will not change when we select alternative groove densities to obtain the 5 and 10 nm WSI values. We find by iteration that a 1,200 g/mm grating provides the reasonable solution shown in Table 1. We also note that the image of the pinhole appears to demagnify in the dispersion plane; however, in these calculations, we assume that the entrance and exit arm lengths are the same, and that the pinhole will change in size only as a function of the cosines of the angles of incidence and diffraction. In an actual instrument, unequal arm lengths are possible and are certainly different across the array. Changing values of Lb with wavelength will contribute to the pinhole magnification.

To summarize the results:

Lb (focal length) = 332 mm.
α (the angle of incidence) = of 26.5° for the wavelength range from 531 to 607 nm.
Diffraction grating = 1,200 g/mm

To select an alternate wavelength range, the grating would be rotated to change the angle of incidence while keeping Lb and the Dv angles constant.

To determine α for a 10 nm WSI, the groove density of the diffraction grating must be four times less than the 1,200 g/mm grating used earlier. By using a 300 g/mm grating, and keeping Lb and the Dv angles constant, we vary α until we reach the desired wavelength range shown in Table 2. Here, the wavelength range from 406 to

Table 2
Estimated Geometric Parameters for a WSI of 10 nm

Eq. (1) (*D*) wavelength range (nm)	Eq. (2) (*C*) β (°)	(*F*) Absolute Dv [From Table 1]	Eq. (12) (*C*) Pinhole (mm)	Eq. (3) Disp (nm/mm)
406	−4.21	−15.46	0.098	10.01
560	−1.55	−12.80	0.098	10.04
717	1.14	−10.11	0.098	10.04

WSI = 10 nm; total length of the IMPT array detector = 32 mm; diffraction grating = 300 g/mm; angle of incidence = 11.25°; focal length 332 mm; pinhole diameter = 100 mm. (*C*) = computed; (*D*) = derived by varying α. Lb and Dv values were fixed in Table 1.

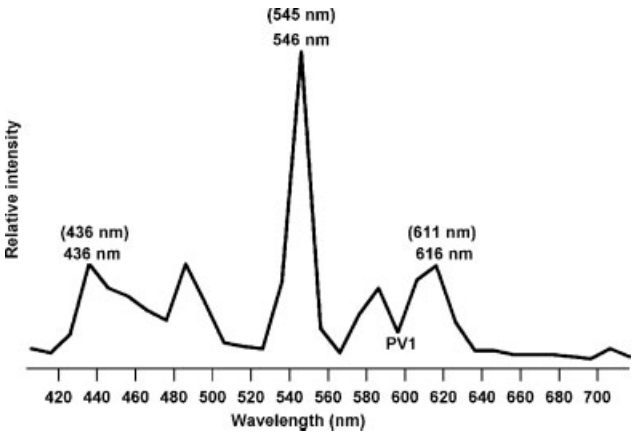

FIG. 8. Nikon C1-Si: simultaneously acquisition of the LightForm MIDL lamp spectrum with a 10 nm WSI. The wavelength accuracy and contrast (peak to valley ratio measured at PV1) are good and well within expectations. It is evident that the image of the pinhole at the Hg 545 nm line strikes a single detector element and the 611 nm line is split between two elements. Values in parentheses are the true wavelength values.

717 nm (311 nm) is acquired in a single shot in 10 nm increments with $\alpha = 11.25°$. The results appear to be consistent with observations.

To keep astigmatism and coma to a minimum, the NA of the system should be kept to a minimum. Astigmatism varies with the square of the NA and coma with the cube of the NA. The projected NA of a 63× objective (NA = 1.32) is 0.02 (1.32/63), and a 10× (0.3 NA) projects at 0.03. If we used a 30-mm wide diffraction grating, the NA of the spectrometer would be 0.05 (*F*/10) and would accommodate the NA of both the high- and low-magnification microscope objectives. In relative terms, an NA of 0.05 is low enough to keep aberrations to a minimum, and the large size of the detector elements will mask whatever residual aberrations remain.

Figure 8 shows an acquisition of the MIDL wavelength calibration lamp with a 10-nm WSI taken in a single shot (see section titled "Wavelength Calibration of Spectral Systems" for details). The emission maxima match the absolute values very well considering that each acquisition was 10 nm wide. The scan also illustrates that, when an image of the pinhole strikes a single detector element, the bandpass measured at the FWHM of the 545 nm peak is indeed 10 nm. However, the 611 nm line clearly falls between two detector elements reducing the apparent FWHM and peak intensity by a factor of two. This is aliasing and is most noticeable when the WSI is large. Although expected, this effect can cause unreliable intensity ratios between wavelengths. Changing the initial wavelength of the scan can push a particular wavelength from one detector to another and change intensity ratios and FWHM values. This is a hazard or an opportunity depending in whether the instrument operator is aware of the consequences of changing a scan starting wavelength.

Note that although we derived a plausible solution there are many variables. For example, Nikon may have used custom diffraction gratings and/or focusing optics; consequently, the actual instrument may have an alternative geometry.

DIFFRACTION GRATING BASED SPECTROMETER SYSTEMS

Spectrometers characterize the spectral characteristics of an object by measuring wavelength intensity as a function of wavelength. Spectrometers work in reflection, transmission, absorption, fluorescence, Raman, and all forms of luminescence and phosphorescence whether chemically or electrically induced. If wavelengths are acquired sequentially by rotating the WDE, then system is a monochromator. If all wavelengths in a specific range are acquired simultaneously, then it is a spectrograph. The spectrometer systems that follow can all be made to operate as a monochromator; however, we are going to focus on spectrograph systems due to their increasing importance to the life science community.

The literature describes a wide variety of spectrometer designs, but we will concentrate on the most common and arguably the most successful. These include the Czerny turner (CT), concave diffraction grating (CDG), and aberration corrected holographic diffraction gratings (ACHG), and prism systems.

As is implied by the above-mentioned list, all spectrographs do not perform equally well. Without implanting specific corrections, spectrometers are subject to field curvature, astigmatism and a variety of off-axis aberrations and anamorphism. Astigmatism does not have a dramatic effect on spectral resolution, but it significantly degrades spatial resolution. Field curvature will not support a linear array, such as an IPMT or a CCD. Of the two, field-curvature is the easiest to correct (15–17).

Field-Flattened Czerny Turner Spectrograph

Most spectrometer systems, such as those found in analytical laboratories, are incapable of determining the location of a spectrum presented by an object in the FOV, and are designed to characterize samples in a cuvette or capillary.

Figure 9 illustrates a CT design that significantly flattens the focal plane to accommodate array detectors, including the previously mentioned Hamamatsu IPMT. A field-flattened CT (FFCT) design is asymmetric, and the focal field is tilted in the wavelength dispersion plane. In this geometry, θ and θ_1 are unequal, and distances La and Lb may also be unequal. Although corrected for focus, spherical aberration, and coma, astigmatism remains a problem; consequently, a FFCT is very well suited to an IPMT with large rectangular detector elements.

Using a Spectrograph with a Linear Array or CCD as a Wavelength Detector

We know that bandpass is a function of wavelength dispersion and the greater of the image of the entrance aperture or the exit aperture Eq. (10). Therefore, the detector element size plays a critical role in determining both spectral and spatial resolution. A linear array, such as the pre-

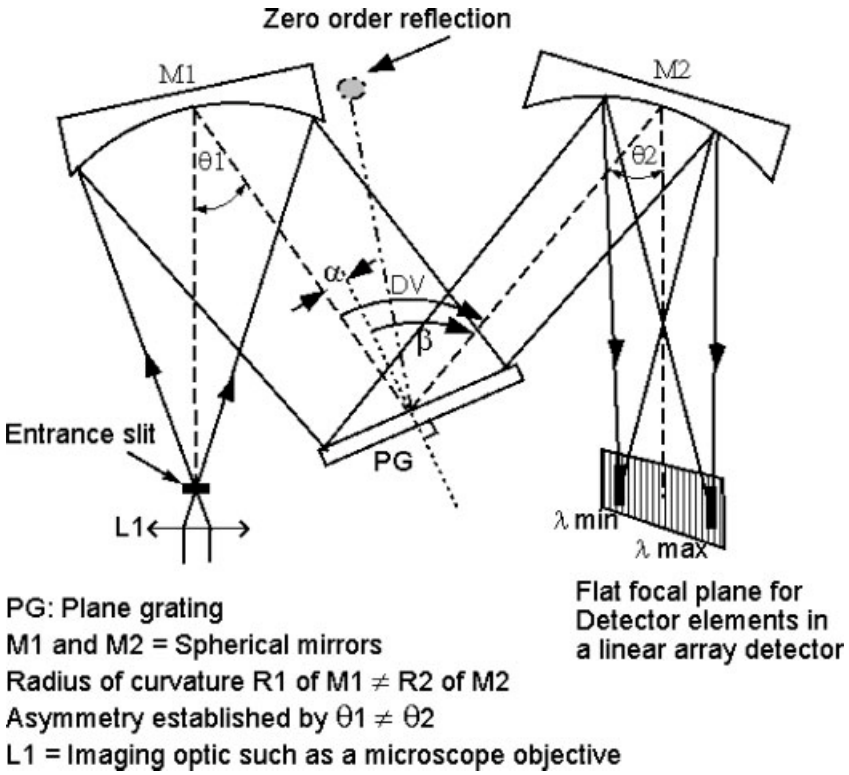

FIG. 9. Asymmetric Czerny Turner designed to flatten a typically curved focal to accommodate an array detector. Residual astigmatism is irrelevant because the height of the detector array captures all incident light and there is no spatial resolution requirement.

viously identified IMPT, has large detector elements and these determine the limits of spectral resolution because the size of the image of the entrance aperture is unlikely to exceed the size of the detector elements.

In comparison, a CCD matrix array, such as the QICAM (Q-Imaging, Burnaby, Canada), is made up of 1,392 × 1,040 μm^2, 4.65 × 4.65 μm^2 detector elements (pixels), each of which provides an individual measure of the amount of light incident upon it. In this example, the pixel size will almost always be smaller than the image of the entrance aperture; consequently, pixel size will not limit spectral bandpass or resolution.

Each spectrum incident on a CCD in an imaging spectrometer will occupy a row (*x*-axis) of pixels and will not produce an "image" that could be likened to a digital photograph. The *y*-axis correlates a position in the FOV with a position on the entrance slit with a spectrum in a row of pixels. If the entrance aperture is a pinhole, then only a few rows of pixels will be illuminated, and the detector should be a linear array, rather than a CCD, because there will be no spatial component.

Astigmatism and Spatial Resolution

Poor spatial resolution is dominantly degraded by astigmatism-an off-axis aberration that increases as the square of both the off-axis angle and NA. Figure 10 illustrates the origins and consequences of astigmatism. Light strikes the WDE in a spectrometer along its width and its height. Rays striking along the width of the object are brought to a tangential focus. The width of the optic is a variable because it depends on the cosine of the angle of incidence, which can vary with wavelength in a monochromator and is a constant in a spectrograph. The height of the optic is not a variable, and rays distributed vertically along the WDE are brought to a sagittal focus. When the sagittal and tangential foci fail to coincide, the system is "astigmatic," and a point object at the entrance slit will be imaged as a line in the exit plane (Fig. 10a).

Astigmatism causes two adjacent points to merge vertically, and the intersection of sagittal edge rays at the tangential focus will determine the height of the astigmatism, as shown in Figure 10a. In this example, each optic has the same radius of curvature (ROC) in both the horizontal and vertical directions, where: $R = Rt = Rs$.

Astigmatism is evident perpendicular to the dispersion axis; consequently, the spectrometer illustrated in Figure 9 can be designed to deliver optimum spectral resolution, but will not deliver good spatial resolution. This is a common design used with a wide variety of linear arrays.

Astigmatism is not a problem in a laser confocal spectral system, because the laser submits single "points" from the FOV sequentially, not multiple points simultaneously. If either an exit slit or detector elements are large enough to catch all available photons, irrespective of how much they are vertically spread or otherwise aberrated, then all energy from each point in the FOV will be captured and quantified. As a result, laser-scanned spectral confocal systems do not have to have an astigmatism-free spectrometer. Similarly, classic spectrophotometers used to characterize a solution in a cuvette use either an exit slit or detector, which is tall enough to collect all vertically distributed light.

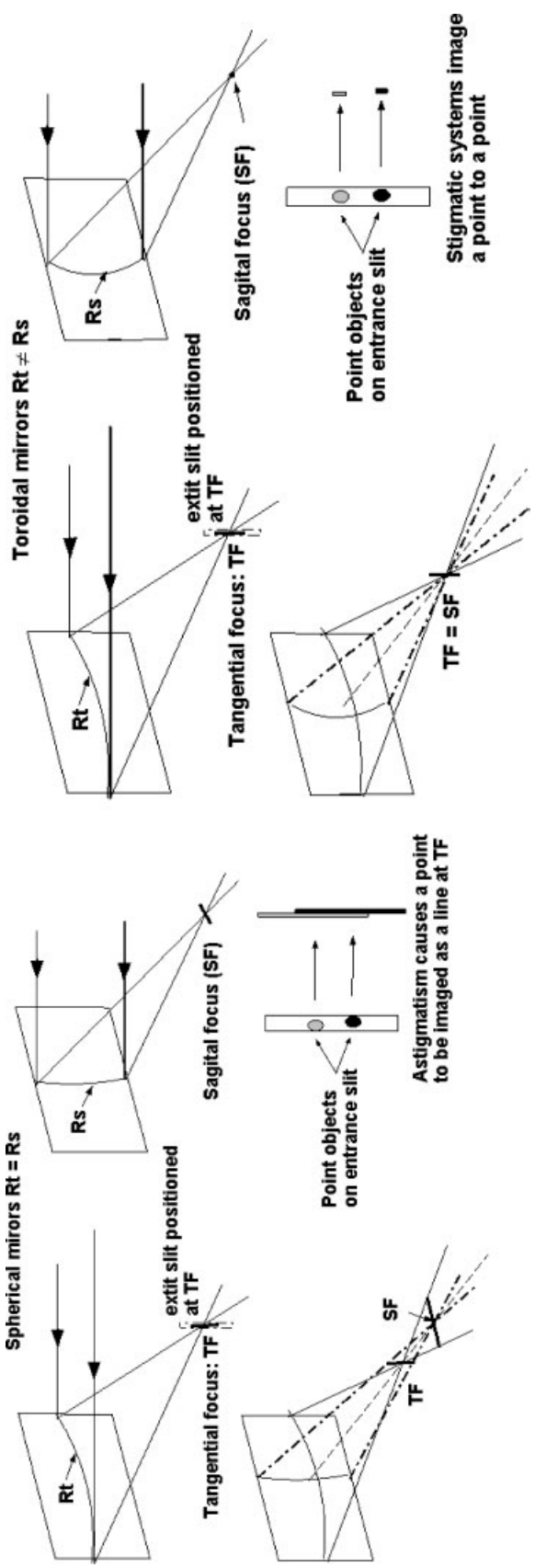

FIG. 10. (**a**) All wavelength dispersive spectrometers operate off-axis resulting in astigmatism that presents a point on the entrance slit as a line at the exit plane. (**b**) Astigmatism can be corrected with toroidal optics with the result that a point on the entrance slit is imaged as a point in the exit plane.

The most obvious solution to the astigmatism problem is to bring the two foci together by making mirrors with a sagittal ROC (Rs) curve that will bend the sagittal focus onto the tangential focus and Rs ≠ Rt. Figure 10b shows an optic with different radii of curvature along the vertical and horizontal axes. The two curves are mechanically ground into the blank of collimating or focusing mirrors, or recorded into the hologram of a holographic diffraction grating.

Astigmatism Corrected CT Spectrometer

Figure 11 shows an example of a nearly stigmatic CT where either the collimating or focusing mirror is a toroid. This is a successful solution that is stigmatic at one wavelength and much improved over a specific wavelength range. It does not work as well when the entrance slit is particularly high, or for a highly extended wavelength range.

A stigmatic spectrometer images points along the entrance slit as spectra with about the same height as a point on the entrance slit. There will be geometric magnification due to differences in the angles of incidence and diffraction (or refraction), Eq. (12) as well as differences in path length along a linear array. Pure 1:1 imaging is impossible at all wavelengths. If the source is monochromatic, then a point will be imaged as a point.

We can assume that a stigmatic spectrometer will use a matrix array, such as a CCD, as the wavelength detector. The actual width of each "point" will be constrained by the height of a row of pixels on the CCD, plus any other residual aberrations that may be present. The greater the number of points on the entrance slit that can be differentiated, the better the spatial resolution and imaging capacity will be.

If a spectrometer is to be used as a source of excitation energy, then astigmatism is a significant problem because the photon density is reduced by any increase in area at the exit of the spectrometer. For illumination or excitation purposes and spectral topographical mapping, the spectrometer should be stigmatic.

Classical Concave Grating Options

Astigmatism is also observed with a classical concave diffraction grating operating on the Rowland circle (RC). The diameter of the RC is the radius of curvature of the grating, as shown in Figure 12. If the entrance slit is located on the RC, then all diffracted wavelengths will also be focused on the RC. The benefit of this configuration is the simplicity of the design, which does not need any collimating or focusing optics and accommodates a very wide spectral range. However, it is not capable of point-to-point imaging because of astigmatism. The considerable field curvature makes the use of linear arrays or CCD chips impractical. This design is widely used in many high-resolution "direct-reading" spectrometers found in analytical laboratories (18).

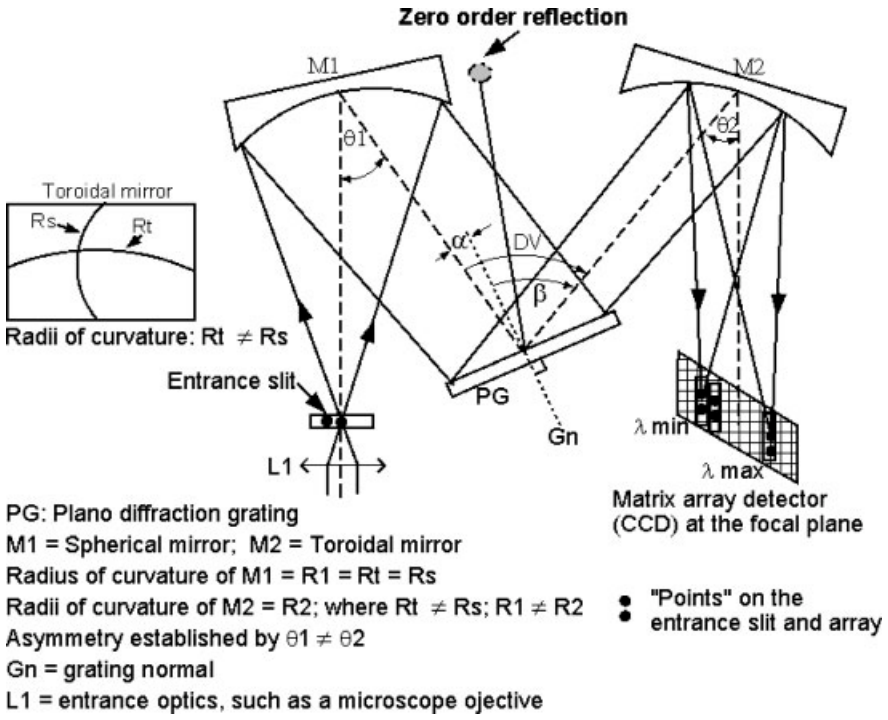

FIG. 11. A toroidal focusing or collimating mirror bends the sagittal focus onto the tangential focus.

Holographic Recording of Aberration-Corrected Concave Gratings

Aberration-corrected holographic gratings (ACHGs) can be recorded in such a way that a spectrum falls on a flat-field with greatly reduced or eliminated astigmatism. No focusing or collimating optics are required and it can be well corrected over a significant wavelength range.

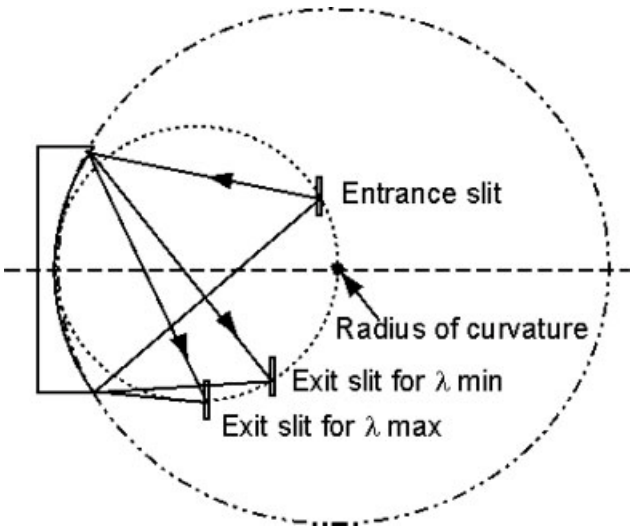

FIG. 12. Concave diffraction grating operating on the Rowland circle (RC). Light entering on the RC will be diffracted and focused on the RC. Spectral resolution is high and it is not capable of spatial resolution due to astigmatism.

The theory behind correcting the aberrations of concave gratings is described in the literature. It is enough to say that a classical concave grating has grooves that are equidistant, whereas ACHG are recorded with asymmetrically distributed grooves, and no longer operate on the RC (Fig. 13). The asymmetry of the grooves is somewhat analogous to using a toroidal optic with asymmetric radii of curvature. For additional correction, the usual spherical grating blank of an ACHG can also be both toroidal and be recorded with asymmetrically distributed grooves (3,6,9, 10,19,20).

Balaban et al. at the National Institute of Health elegantly demonstrated the use of an ACHG flat-field spectrograph grating (UFS 200, Horiba Jobin-Yvon) in 1985, by generating fluorescence spectral acquisitions across the nucleus of a living trophoblast cell, using a SIT matrix array camera as the wavelength detector (21).

By 1990, Benedetti and Evangelista at the Instituto di Biofisica in Italy used a more advanced ACHG flat-field spectrograph grating (Horiba Jobin Yvon ref model 52300070) coupled to a CCD detector to perform spectroscopic, slit-confocal microscopy. A conventional confocal system takes a point excitation at the sample and reimages it onto a circular aperture, whereas in this case, the sample was excited by a "line" of light, rather than a point. The areas of the sample that fluoresced under the influence of the line excitation were projected onto the slit of the spectrometer to make a slit-confocal spectral microscope, thereby, reducing scatter and enhancing contrast. The full spectral data from each point along the slit was captured simultaneously (as illustrated in Fig. 13), and the sample was translated sequentially until the entire FOV was acquired. Software then reconstructed the spectral information into a spectral topographical map (22).

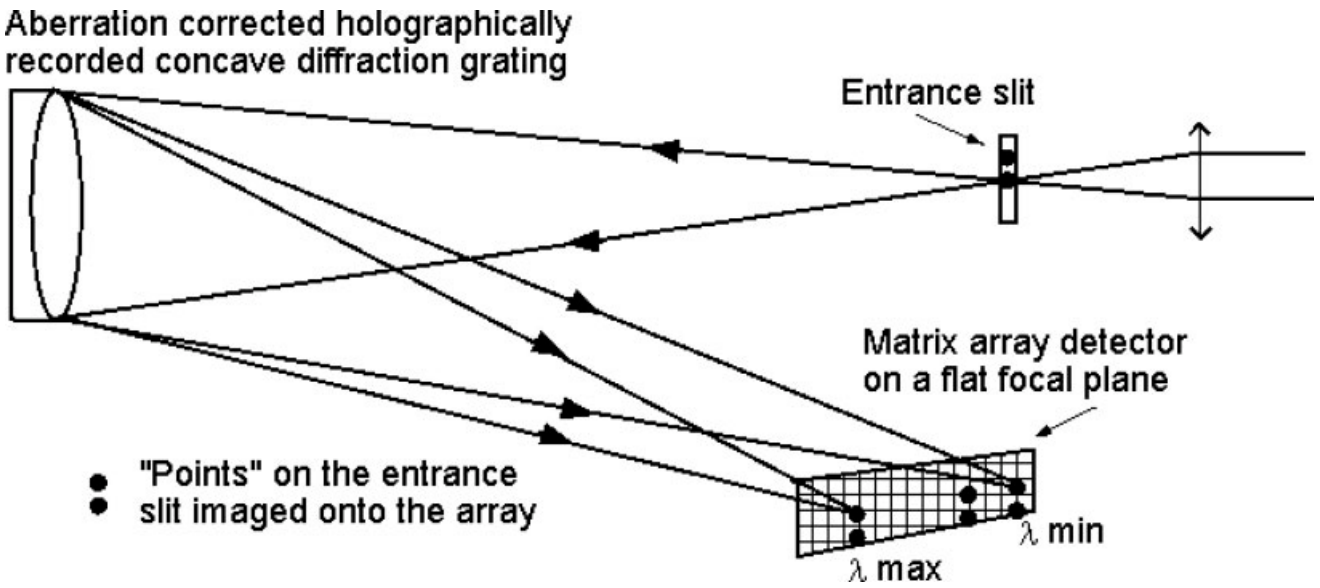

FIG. 13. Holographically aberration-corrected concave grating spectrometer. This solution does not require any ancillary collimating or focusing optics.

PRISM-BASED SPECTROMETER SYSTEMS

Classical Prism Spectrometer Designs

Figure 14 shows a generic wavelength dispersive prism system with a typically curved focal field. Optic CO collimates light from the FOV onto the prism at an angle α. After refraction, each wavelength exits at an angle β. The similarity to a diffractive system is self-evident with the same influences that contribute to aberrations. However, prisms only refract a single order; consequently, light transmission efficiency can be very high and only depends on the wavelength and the material that is used to make the prism.

The most effective means to collimate and focus light in any wavelength dispersive system is with front surface concave mirrors; however, in order to produce a more compact system, lenses are often used at CO and FO. Finding lenses that are transmissive over all wavelengths, field flattened and chromatically corrected to spectroscopic standards, and also able to correct astigmatism present in the off-axis refracted light, can be a challenge. Consequently, it is not unusual to find a variety of residual aberrations, including astigmatism, coma, and spherical aberration in the focal field.

This or a similar prism geometry is probably used in the Leica SP series spectral confocal microscope, using the confocal pinhole as the entrance aperture of the spectrometer. The system does not need elaborate aberration correction, because the image of the pinhole is imaged not onto another circular aperture, but a slit. Any astigmatism is accommodated by making the exit slit high enough to capture any vertical image enlargement. This works because the laser excites the sample point-by-point sequentially; so that there are never two objects being imaged at the same time that could interfere with each other. To acquire a complete spectrum, the exit slit is

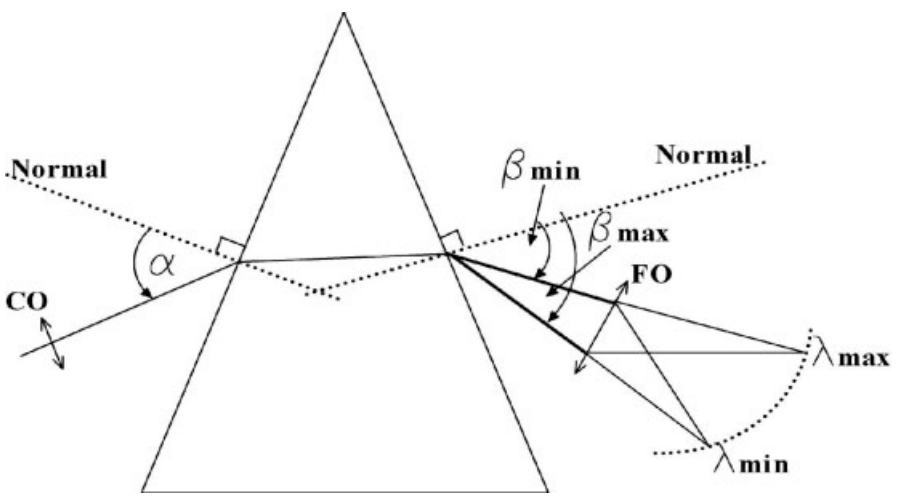

FIG. 14. Generic wavelength-dispersive prism system.

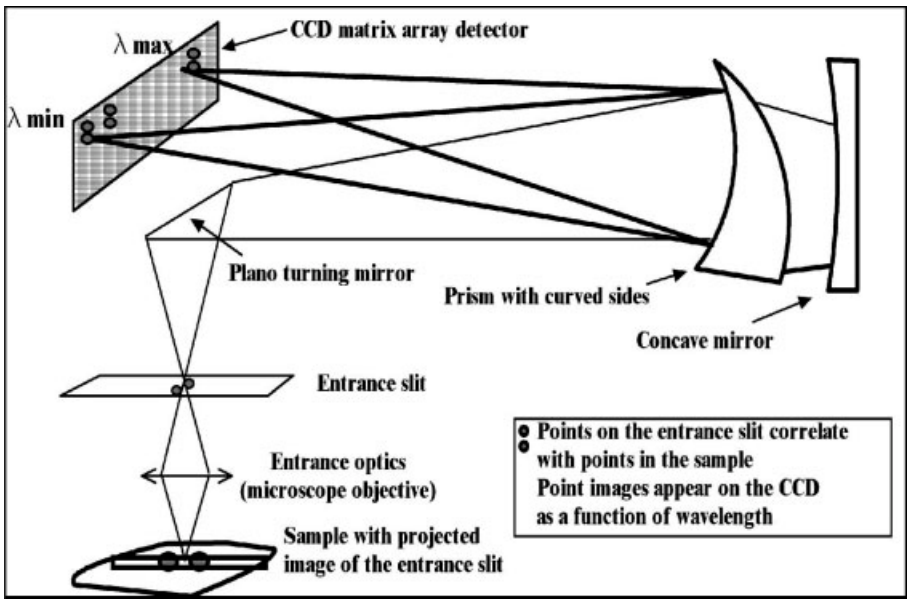

FIG. 15. PARISS aberration-corrected prism-based spectrometer.

translated across the focal field and a single PMT measures the signal at each wavelength.

An Aberration-Corrected Prism-Based Imaging Spectrometer

In 1989, Warren and Hackwell, at the Aerospace Corporation in El Segundo, California, developed a highly aberration-corrected, prism-based spectrograph. Originally called *SEBASS*, and designed for use in the wavelength range 2.9–13.5 μm, it used a telescope for light collection and a matrix array as the detector. After LightForm acquired the license to the patent, it was redesigned for use in the wavelength range from 360 to 950 nm, and named "PARISS" (prism and reflector imaging spectroscopy system). PARISS was optimized for use in fluorescence, absorption, and reflection microscopy with a digital CCD as the detector (Fig. 15). PARISS acquires all wavelengths in the wavelength range from 400 to 800 nm simultaneously over a ½-inch CCD chip and from 365 to 800 nm over a conventional 2/3rd inch chip (23,24).

This novel design uses a front surface concave mirror at finite conjugates (to create an image of an object) with a small off-axis angle, and a highly optimized, computer designed prism, with concave and convex sides. The combination of curves and distances from optic to optic produces an almost aberration-free flat focal plane that accommodates a digital CCD camera. The curved sides of the "prism" makes it closer to being a lens with a wedge. The design is made highly resistant to reflections and ghosting by tilting the optical components so that no optic "looks" directly at any other. In this way, any reflections pass harmlessly out of the optical path, and never reach the detector. The light transmission efficiency over the design range is >90% in the visible, and is capable of true point-to-point imaging over a wide FOV. Figure 16 shows the spectrum of a low-pressure Hg calibration lamp spectrum from 365 to 950 nm acquired on the PARISS system, with a single 10 ms exposure, using a CCD detector with a 1-inch CCD chip (Retiga 2000R with 2 × 2 binning, Q-Imaging Corp, Burnaby, BC, Canada) (see section titled "Wavelength Calibration of Spectral Systems" for details). The measured bandwidth of the 436 nm line is 1 nm. Although it is not obvious, this spectrum is remarkable because Argon lines above 650 nm fade to extinction within seconds of turning on the lamp. The fact that the Hg 365 nm line and the Ar 912 nm line are both captured simultaneously highlights the power of a prism to rapidly capture a very wide wavelength range with no contaminating higher orders.

Spectral Resolution and CCD Pixel Density

The number of pixels in a CCD chip, when used as a wavelength detector in the focal plane of a spectrograph, has a very limited bearing on spectral resolution. The spectral resolution for a slit-based instrument is governed by the generalized bandpass Eq. (11). Consequently, the spectral resolution in the dispersion plane (*x*-direction) is a function of the width of the slit and in the spatial (*y*-direction) is governed by the height of a row of pixels on the CCD. In both cases, residual aberrations, magnification, and the natural energy distribution (atypically Gaussian) will each contribute to image enlargement.

For example, let us take the previously mentioned QICAM with 1,392 × 1,040 pixels each of which is 4.65 × 4.65 μm^2 in size. We know that an image of the entrance aperture is imaged onto the CCD at all wavelengths present in the emitting source simultaneously. As a practical example, the PARISS system uses a 25 μm entrance slit width, 5 mm in height and its operating geometry (La < Lb) magnifies the width and height of the entrance slit by ~10% resulting in an ~27 μm wide image of the entrance slit. This corresponds to an observed bandpass of 1 nm, FWHM,

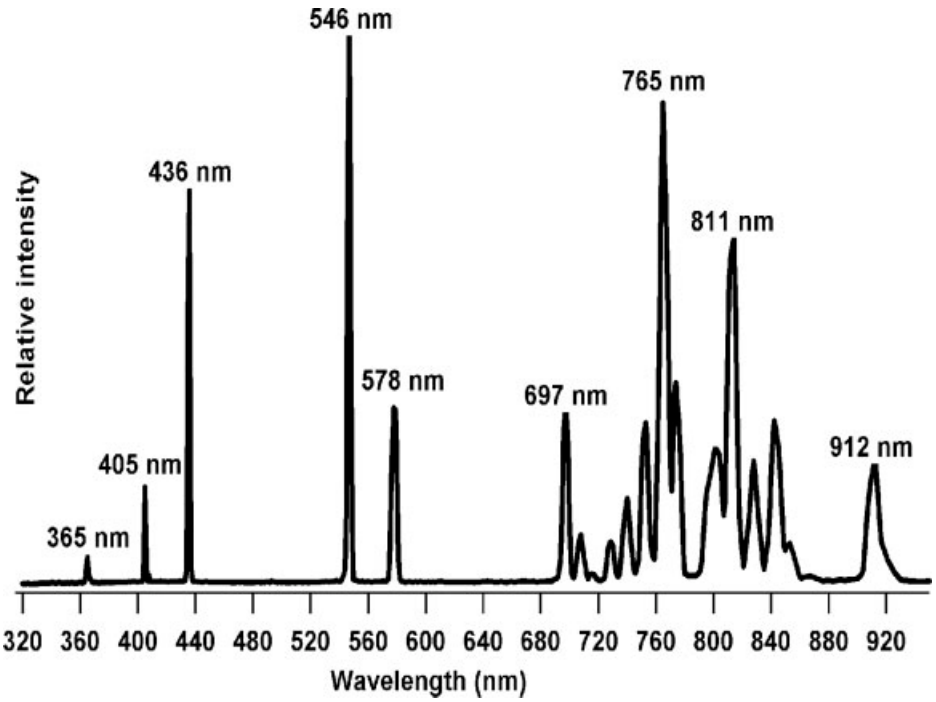

FIG. 16. Wavelength calibration spectrum of a low pressure Hg lamp. All wavelengths were acquired simultaneously with the PARISS system using a Retiga 2000R with a 2/3rd inch chip. The emission lines above 650 nm are Ar^+ lines that have a very brief lifetime after the lamp is turned on.

at the Hg 436 nm line. Therefore, the linear dispersion of the PARISS system at 436 nm is 37 nm/mm.

For a monochromatic emission wavelength, we know that bandpass is the linear dispersion multiplied by either the width of the image of the entrance slit or the exit aperture, whichever is larger. However, because we are using a CCD, we can select the number of pixels that will accommodate the image of the entrance slit. Given that each pixel is 4.65 μm in width, the image of the entrance slit will occupy 6 pixels (the integer value of 27/4.65). However, by the Rayleigh criterion, we only need three data points to define the FWHM, so that there will be no loss in spectral resolution by binning pixels 2 × 2 and we will benefit by an increase in linear dynamic range, and signal-to-noise ratio. It is also demonstrable that there was no measurable image enlargement apart from the expected geometric magnification.

Spatial Resolution and CCD Pixel Density

The spatial resolution in the dispersion plane, at the CCD, is given by the entrance slit width divided by the magnification of the light collection optic imaging the sample, such as the microscope objective. For example, if we image an object in the FOV with a 40× objective onto a slit 5 mm in height by 25 μm in width, then the spatial resolution at the sample will be 25 μm divided by 40× = ~0.6 μm at an object's FWHM. In theory, a 100× lens should give us a spatial resolution of 0.25 μm; however, depending on the wavelength of light, diffraction effects, and residual aberrations (from the microscope objective, the spectrometer, and wavefront errors through relay lenses and filters), the practical FWHM spatial resolution will most likely plateau around 0.4 μm. It is also unlikely that the image of any object will strike only 1 pixel on the chip; so it is to be expected that the spatial resolution will be moderated at least by the Gaussian spread of the image at the entrance slit.

At the CCD chip (where the image of the entrance slit is located), the spatial resolution along the slit height (*y*-axis perpendicular to dispersion) is again limited by the height of a single row of pixels and the Gaussian energy in a point object. After binning to match the width of the entrance slit, the vertical resolution also approximates ~0.6 μm with a 40× microscope objective. Therefore, we will observe up to 240 spectra along the slit, corresponding to 240 objects, ~0.6 × ~0.6 μm^2 in size, distributed along a linear slice of the FOV. If objects in the FOV are true point sources, such as nanoparticles or single molecules, then if only one such emitter is imaged through the slit, the slit acts as a field aperture. The image of the point source effectively defines the entrance aperture and will fill one (or partially two) rows of pixels. The accuracy of the location of the point object in the FOV will continue to be 0.6 × 0.6 μm^2.

Spatial resolution is only limited when the object is extended in size. If the image of an object is smaller than the slit width, then it is the image of that object that acts as the entrance aperture.

Generating Spectral Images with a Wavelength Dispersive Imaging Spectrometer

When we take a digital photograph with a CCD camera, we acquire a fixed FOV that is characterized pixel-by-pixel in the array. If we take an image of the same FOV through a series of WDP through wavelength bandpass filters, we would generate a stack of as many images as there are WDPs. Each pixel will contain a "spectrum" consistent with the number of WDP in the series. Motion of objects in the

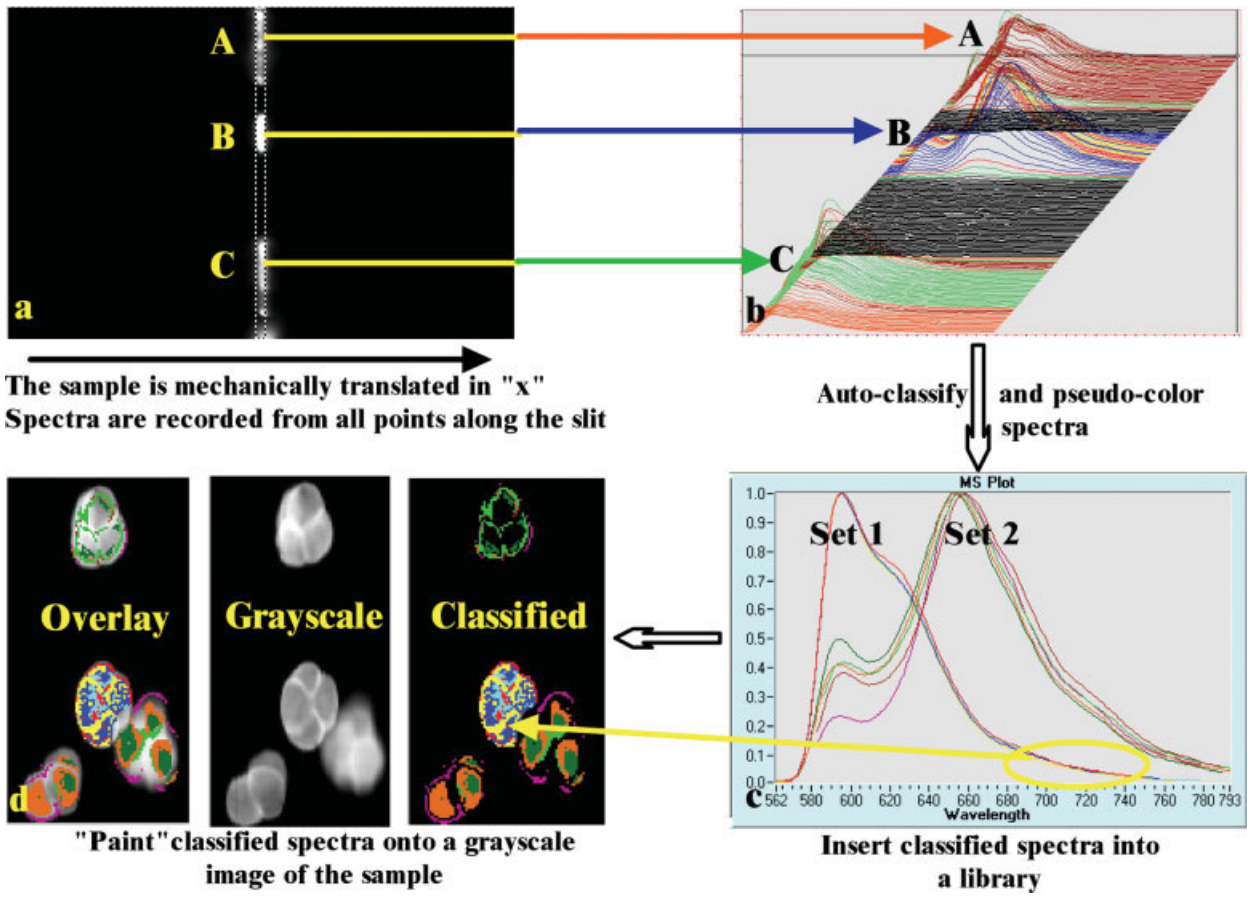

FIG. 17. Classification and spectral mapping of the fluorescence spectra of pollen grains (pollen was chosen for the wide range of fluorescence signatures present). (**a**) A rectangular section of the FOV is allowed to pass through the entrance slit. (**b**) Spectra from points in the FOV incident on the entrance slit. (**c**) The spectra in the FOV are sorted into classes and inserted into a library. There are three spectra in Set 1, pseudocolor coded blue, yellow, and red; Set 2 has five spectra. (**d**) Correlated spectra painted onto a grayscale image of the FOV. Note how the three spectra in Set 1 differentiate in the spectral image of the FOV. Areas in gray do not correlate with any library spectrum.

FOV or a chemical reaction during the time it takes to acquire the full WDP series will compromise the integrity of the spectra. A filter-based approach takes a fixed FOV simultaneously, and wavelength acquisitions sequentially.

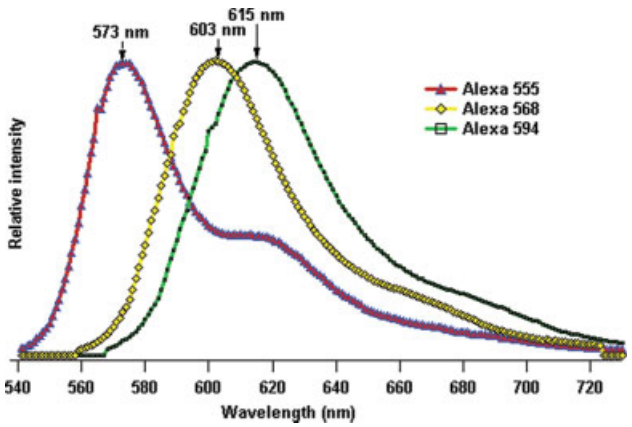

FIG. 18. Spectral characteristics of Alexa 555, 568, and 594 acquired on the PARISS spectral imaging system as observed within a tissue section shown in Figure 19.

In a wavelength dispersive system, using a CCD camera as a detector, the process is reversed. A spectrograph submits all wavelengths present in an object simultaneously

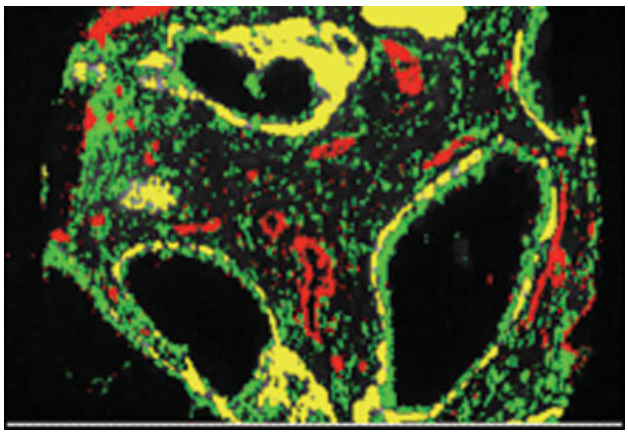

FIG. 19. Spectral topographical map of Alexa 555, 569, 594 in a tissue section acquired on the PARISS spectral imaging system. A pseudocolor was assigned to each of the dyes. Correlated spectra were "painted" onto a grayscale image of the tissue section with pixel perfect accuracy.

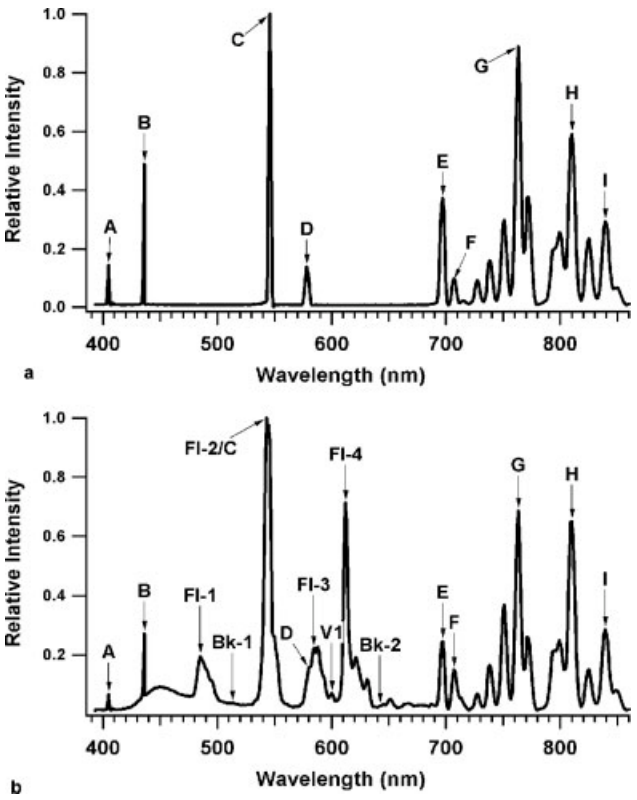

FIG. 20. Spectra of two calibration sources: (**a**) pure Hg/Ar low-pressure discharge lamp; (**b**) LightForm multi-ion discharge lamp (MIDL). Both spectra are as presented and digitized by the PARISS spectrometer.

to the detector. However, the entrance slit in this case acts as a field stop by limiting the area of the FOV passing through the spectrometer. To generate an image, the FOV must be translated sequentially. Remote earth-sensing imaging spectrometers mounted in a satellite or aircraft create spectral topographical maps by "flying over" an unlimited FOV.

It is the same principle in a microscope system. Here, the sample is translated in the *x*-direction in increments consistent with the slit dimensions. If the slit is 25 μm wide and 5 mm in height, and objects are viewed through a 40× objective, then the area of the FOV submitted to the detector is 0.625 × 125 μm^2 (25/40, 5,000/40) and the sample would be translated in 0.625 μm increments. To create an image, spectra collected from the FOV are categorized into "classes" where each class correlates with an object, condition, or interaction. A library of the classes of spectra stores pseudocolor codes for each class. Each time a spectrum from the FOV correlates with a particular class of spectrum, to a user defined threshold, it is "painted" onto the FOV in its associated pseudocolor. Figure 17 is a general schematic of the process. Figure 17a shows that only a slice of the FOV is acquired in a single acquisition. The FOV is mechanically translated across the projection of the entrance slit in the FOV. In Figure 17b, each acquisition records all wavelengths simultaneously with as many spectra as there are rows of pixels on the camera (sometimes after binning). Figure 17c shows classified spectra from the FOV that have been inserted into a spectral library, each with a user assigned, unique color-code. In Figure 17d, all newly acquired spectra that correlate to library spectra, at a user defined threshold, are painted onto a grayscale image of the FOV. The colors are the same as those that the user assigned in the spectral library. Because the FOV is mechanically translated, there is no limit to the extent of the field that can be spectrally mapped.

Figure 18 shows the spectral characteristics of Alexa 555, 568, and 594 that was used to fluorescently label a tissue sample. The dyes were pseudocolored red in areas corresponding to Alexa 555, yellow to Alexa 568, and green to Alexa 594. Figure 19 shows the spectral topographical distribution of the Alexa fluorophores acquired with the PARISS system. All wavelengths were acquired simultaneously over the wavelength range from 540 to 720 nm. Whenever an acquired spectrum correlated with that of one of the Alexa dyes, its assigned pseudocolor was painted with pixel perfect accuracy onto a gray scale image of the tissue section.

WAVELENGTH CALIBRATION OF SPECTROMETER SYSTEMS

Wavelength accuracy is best determined with a low-pressure Hg^+/Ar^+ discharge lamp that covers the wavelength range from 365 to 850 nm. The emission spectrum of this lamp from 400 to 842 nm is shown in Figure 20a. ("Spectroline," Spectronics Corp., Westbury NY, and Oriel Corp., Stratford CT supply a wide variety of wavelength calibration lamps.) The main drawback of pure Hg^+/Ar^+ lamps is that they emit deep UV light that is dangerous to exposed skin and can cause blindness to unprotected eyes. Consequently, we use an eye-safe, multi-ion discharge lamp (MIDL) distributed by LightForm, Inc. (Hillsborough, NJ). The MIDL presents monochromatic emission features emitted by Hg^+, Ar^+ as well as narrow, but not monochromatic, inorganic fluorophores to cover the spectrum from 400 to 840 nm, as shown in Figure 20b. The lamp actually emits down to 365 nm, but the 365 nm

Table 3
Peak Maxima for Principal Spectral Features in the MIDL Calibration Light Source

	Wavelength	Emission
A	404.7	Hg
B	435.8	Hg
C	546.0	Hg
D	577/579	Hg
E	696.5	Ar
F	763.5	Ar
G	811.5	Ar
H	842.0	Ar
F1-1	485.0	Fluorophore
F1-2	544.0	Fluorophore
F1-3	586.0	Fluorophore
F1-4	611.5	Fluorophore
V1	605.0	Valley
BK1	525	Background
BK2	642	Background

Hg line is weak in this lamp (for eye safety), and is not shown here.

The MIDL lamp is battery operated and emits light from a 6-mm diameter "pencil" tube that replaces the sample on the microscope stage. Table 3 shows selected Hg^+, Ar^+, and fluorophore emission features corresponding to the letters in Figures 20a and 20b.

The benefit of an MIDL spectrum is that it emits a spectral fingerprint that can be used to calibrate the performance of any spectroscopic system. (A full listing of wavelength emission features can be obtained from the National Institute of Standards and Technology (NIST) (25).) Most importantly, however, an MIDL can be used to compare the performance of any instrument with any other and validate the accuracy of wavelength data (26).

PRACTICAL APPLICATIONS OF THE SPECTROMETER MATH TO PREDICT THE AREA OF A LASER "SPOT" AT THE SAMPLE

Spot Size and Pinhole Optimization

Probably one of the most discussed issues in confocal microscopy are the questions, "what is the true spot size at the sample?" and, "what can I expect when the pinhole is opened?" The literature informs us in great detail how to calculate the size of an Airy disc produced by the laser at the sample, and transmit it through the confocal optics until it passes through the pinhole. All good theory, but it is possible to test what happens in reality for any given sample.

Looking at the problem from a geometrical optics point of view, the amount of light passing to the detector must obey the Etendue Eq. (9). If the pinhole is perfectly matched in size to the projected image of the Airy disc at the sample, then all available light should pass through the system to the detector. If there is no scattering, signal will increase for as long as the image of the Airy disc is greater than the size of the pinhole, and then form a plateau when the pinhole is larger than the image of the Airy disc.

If the spot size at the sample is large due to scatter, or other less obvious reasons, then we can expect an increase in the size of the projected image of the spot and it will overfill the pinhole. If the pinhole is homogenously overfilled, then we can expect an increase in signal that will vary as the square of the diameter of the pinhole, until finally the pinhole is larger than the spot size, at which point it should again form a plateau.

We tested this experimentally on a Leica SP1 spectral confocal microscope (LCSI).

Estimation of Illuminated Area of a Laser-Excited Sample

The LCSI system uses a prism as the WDE and the confocal pinhole forms the entrance aperture to the spectrometer. A spectrum is acquired wavelength-by-wavelength by sequentially translating an exit slit assembly along the focal field. It seems evident from the results that the width of the exit slit tracks the nominal width of the pinhole. A spectrum is acquired in 5-nm steps or wavelength sampling increments (WSI).

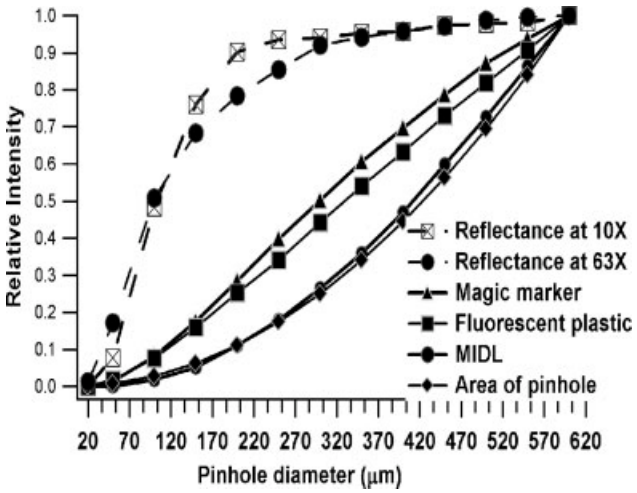

FIG. 21. Intensity versus pinhole diameter for various samples. Note that the MIDL curve closely follows the curve for the area of the pinhole, as predicted by Eq. (9). The plots for the mirror form a plateau after twice the size of the Airy disc using the 10 and 63× objectives, indicating that the Airy disc determines the illuminated area of the pinhole. In the case of magic marker and thick fluorescent plastic, as the pinhole is opened signal continues to increase well past the size of the Airy disc and never forms a plateau. This proves that, with these two sample types, the size of the Airy disc does not correspond to the illuminated area of the sample. It also indicates that the bandpass will vary with the size of the pinhole. Leica 10×, 0.4 NA objective was used unless otherwise indicated.

Figure 21 shows a series of plots in which the curve with diamonds is simply a plot of the normalized area of the pinhole. If we have a perfectly homogenous extended light source evenly illuminating the pinhole, then we would expect that transmission curve to exactly follow the area of the pinhole as predicted by the Etendue Eq. (9). If the sample is truly a small "point," then we would expect the curve to rise until the pinhole is larger than the image of the spot and then plateau.

We tested the principle first with an example where there is no Airy disc and the sample can be considered to be an "infinitely" scattering extended source. We chose the emitting area of an MIDL fluorescent calibration lamp for this purpose because it was certain to fully and homogenously illuminate a pinhole opened to its maximum extent.

All the following acquisitions were made using a 10× objective. Using a fluorescent MIDL calibration lamp (monitored at one wavelength) as an extended source, we indeed observe that as the pinhole is opened the curve closely follows the area of the pinhole as expected and as shown in red circles.

To compare this with a rigorously nonscattering sample, we imaged the laser on a front surface mirror and incrementally opened the pinhole. Again we observed that, as expected, the slope of the light throughput curve rose rapidly and then formed a plateau. We tried this with both a 10× (red squares with an "X" within the box) and a 63× objective (blue circles) with essentially the same result.

We then selected samples that would be more likely to scatter light. The first of these samples was a produced by drawing a very thin line of magic marker on a glass slide and exciting it with a 488 nm laser, focused to maximize signal with the smallest pinhole size. We incrementally increased the pinhole diameter and observed that the throughput curve, shown with triangles, did not follow either the pure reflector model, suggested by the front surface mirror, or the extended source model suggested by the calibration lamp. However, it was much closer to the extended source model than we expected.

We repeated the experiment with a thick fluorescent plastic slide and found that the curves for both the magic marker (triangles) and the plastic slide (squares) were the same up to a pinhole size of ~150 μm (corresponding to two Airy discs) and then as the pinhole increases in size, the slopes of the two curves begin to diverge, with the thick plastic slide tending more toward the curve plotting the area of the pinhole than that of the magic marker.

Neither the plastic slide nor the magic marker followed the intensity curve as a function of the area of the pinhole, indicating that the pinhole is nonuniformly filled and the area of excitation at the sample is neither a "point" nor a homogenously extended illuminated area (such as an MIDL).

The fact that it appears that even with a supposedly nonscattering sample, such as the magic marker, the apparent illumination of the pinhole is greater than the pinhole size. Consequently, increasing the size of the pinhole will result in an increase in light intensity according to Eq. (9) and a decrease in spectral bandpass according to Eq. (10).

Degradation of Bandpass with Increasing Magnification and NA

In the case of a laser confocal system, from Eq. (9), we know that the size of a pinhole should be matched to the size of an Airy disc, and the size of the Airy disc is a function of the magnification of the lens and the NA. It may be counter-intuitive, but while the spatial resolution may increase as a function of magnification and NA, spectral resolution decreases with the size of the Airy disc (27–30).

$$R_{\text{opt}} = A\,\lambda M/\text{NA} \qquad (14)$$

where: R_{opt} is the pinhole diameter; A, a constant; λ, wavelength; M = magnification; NA, numerical aperture

Bandpass reminder: BP = linear dispersion × the exit slit width (or the image of the entrance aperture, whichever is greater).

To compare the diameter of the Airy disc at 10×, NA = 0.4 lens with a 63×, NA = 1.32 lens we only have to take the ratio of magnification (M) to NA in Eq. (14). The nominal ratio for the 10× lens is 25, and ~48 for the 63× lens keeping A and λ constant. The increase in pinhole diameter will be 48/25 = 1.9. Consequently, from Eq. (10), we can expect spectral resolution and bandpass to degrade by approximately by a factor of two when using the 63× lens compared to the 10× lens.

Table 4
Pinhole Diameter Versus Airy Pinhole Number (Leica SPI) for a 10×, Plan Apo, NA = 0.4

Pinhole diameter (μm)	Pinhole number
80	1
156	2
241	3
319	4
397	5
475	6
558	7

To determine the agreement between the theoretical predictions of the generalized bandpass Eq. (11) and the observed spectral bandpass as the pinhole diameter increases, we ran a wavelength scan using the MIDL as a light source between 520 and 580 nm to capture the 544/546 Eu/Hg lines on the Leica SP1 system. We varied the pinhole diameters as shown in Table 4. Figure 22 shows an overlay of the spectral scans for pinholes 1, 4, and 7 corresponding to pinhole diameters of 80, 319, and 558 μm.

Comparison of Observed Versus Theoretical FWHM with Increasing Pinhole Size

For a real life experiment with an emitting source with finite bandwidth we can use the generalized bandpass Eq. (11) to determine the theoretical bandpass BP_{net}. First, however, we need values for the five terms W_{exap}, BP_{nat}, BP_{res}, BP_{slit}, and wavelength dispersion (Disp).

W_{exap}: We take the actual size of the pinhole with the initial assumption that the image of the entrance pinhole is matched to the width of the exit slit. If the width of the slit is not matched to the width of the image of the pinhole, this will become apparent when we correlate theory with observation.

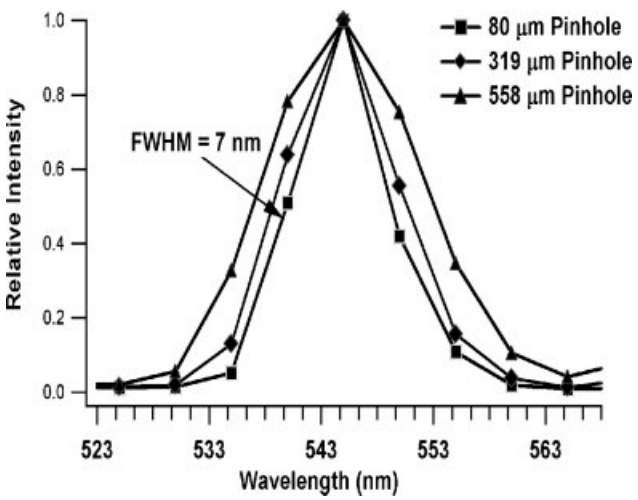

FIG. 22. Pinhole diameter versus bandpass. Using the MIDL lamp as a light source, the FWHM of the 545 nm spectral feature increases nonlinearly, but predictably, as the pinhole diameter increases. This data were acquired on a Leica SP1 spectral confocal microscope.

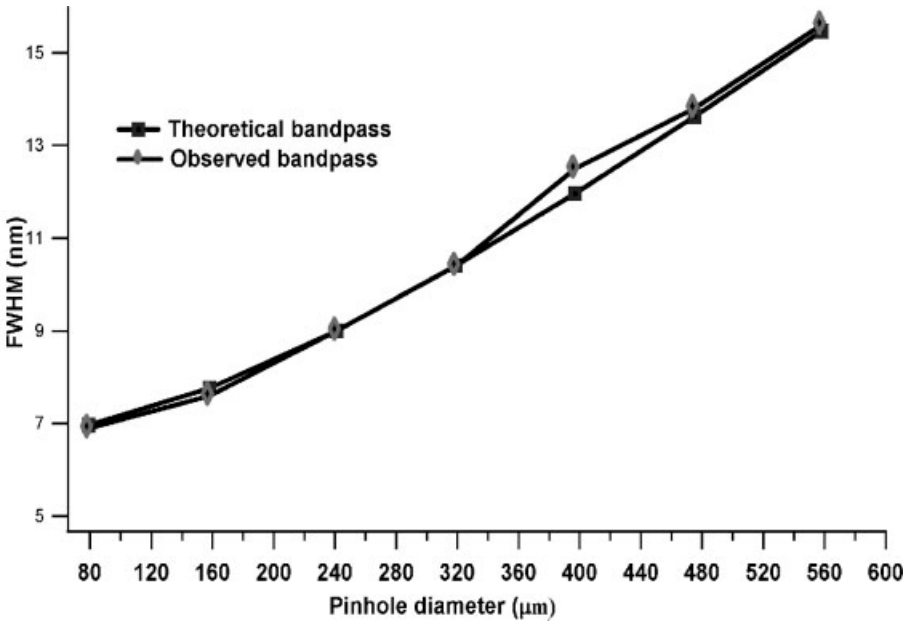

FIG. 23. Observed and theoretical plots of bandpass versus pinhole size at 545 nm (the midway point between the 544 nm Eu fluorescent maximum and the 546 Hg line). Note that the agreement is excellent.

BP_{nat}: The emission band centered at 545 nm is a composite of the Hg 546 nm line (which is essentially monochromatic) and an inorganic fluorophore peaking at 545 nm; the composite FWHM is 4.75 nm (measured from a high-resolution spectrum of the MIDL lamp on the previously mentioned Mechelle, spectrograph).

BP_{res}: Using basic optical principles, for a flint glass prism spectrometer, and focusing optics consistent with the size of the Leica spectrometer box, we expect a limiting resolution between 4 and 7 nm. We iterated the terms BP_{res} and BP_{slit} in the generalized bandpass equation to determine that the closest fit for BP_{res} was 4.7 nm.

Disp: Leica does not supply this information; therefore, the dispersion value was estimated by iterating until the theoretical BP_{net} corresponded to the observed BP_{net}. The calculated value that produced the closest fit was 25 nm/mm at 545 nm.

BP_{slit}: This is calculated from Eq. (10) by multiplying the deduced dispersion by the pinhole size (W_{exap}). By using 4.7 nm for BP_{res} and 25 nm/mm for the wavelength dispersion at 545 nm, we obtain an almost perfect fit with the observed FWHM values, as shown in Figure 23. Bandpass is seen to degrade more or less linearly with pinhole diameter. The excellence of the fit with the theoretical FWHM also indicates that either the width of the exit slit is always matched to the size of the pinhole or that the image of the pinhole is always greater than the effective width of the slit. We can expect to see the same degradation in bandpass whenever the pinhole size is increased on this instrument. Any system using detector elements that are always larger then the image of the pinhole will show no change in bandpass as a function of pinhole diameter. This is because bandpass is determined by the larger of either the image of the pinhole of the exit width aperture width. When using an IPMT, the exit aperture is the width of a single detector element [Eq. (10)].

It is evident that there is very good agreement. This confirms that expectations predicted by the bandpass and Etendue equations are powerful tools in predicting instrumental performance.

CONCLUSIONS AND SUMMARY

We have seen that the design and implementation of a spectrometer has a profound effect on its ability to determine either the spectral characteristics or the location of an object in a FOV. Best imaging is achieved when an object in the FOV is illuminated or excited by a point source. When accurate spectral imaging is required over a large area of the FOV, the spectrometer must be capable of meeting the nontrivial challenge of point-to-point imaging.

Understanding the equations that govern the bandpass and wavelength dispersion of light enables a researcher to optimize light throughput, and understand the true emission characteristics of an object. We also illustrated how the operating parameters of a spectral confocal system can be estimated starting with some simple observations, and how to determine the true illuminated area of an object in the FOV. With a monochromatic line emission source such as an Hg or MIDL lamp, we can measure wavelength accuracy and residual instrumental aberrations, as well as the relationship between aperture size and spectral resolution.

ACKNOWLEDGMENTS

Thanks to Robert Zucker of the USEPA for running the Leica SP1 experiments. The copyright to the spectra shown in Figure 18 are owned by Molecular Probes Inc., probes.introgen.com. Thanks to Dr. Michael Donovan at Aureon Corporation for permission to reproduce the Alexa stained tissue section in Figure 19, and David Cook of Spectrum Scientific Inc., for his suggestions concerning volume transmission diffraction gratings.

LITERATURE CITED

1. Dickinson ME, Bearman G, Tille S, Lansford R, Fraser SE. Multi-spectral imaging and linear unmixing add a whole new dimension to laser scanning fluorescence microscopy. BioTechniques 2001;31:1272–1278.
2. Garini Y, Katzir N, Cabib D, Buckwald RA, Soenksen DG, Malik Z. Spectral bio-imaging. In: Wang XF , Herman B, editors. Fluorescence Imaging Spectroscopy and Microscopy. New York: Wiley; 1996. p 87–124.
3. Hutley MC. Diffraction Gratings. London: Academic Press; 1982.
4. James JF, Sternberg RS. The Design of Optical Spectrometers. London: Chapman & Hall; 1969.
5. Lerner JM, Thevenon A. The Optics of Spectroscopy: A Tutorial. Metuchen NJ: Jobin Yvon/JY Optical Systems; 1998.
6. Loewen EG, Popov E. Diffraction Gratings and Applications. New York: Marcel Dekker; 1997.
7. Stroke GW. Diffraction gratings (in English). In: Flugge S, editor. Handbuch der Physik XXIX. Berlin: Springer; 1967.
8. Lerner JM. Ruled and holographic gratings: A historical perspective. Proc SPIE 1995:2532;2–14.
9. Lerner JM, Chambers RJ, Passereau G. Flat-field imaging spectroscopy using aberration corrected holographic gratings. Proc SPIE; 1981:268; 122–128.
10. Flamand J, Labeyrie A, Pieuchard G. Diffraction gratings. US Pat. 3,628,849, 1971.
11. Flamand J, Bonnemason F, Thevenon A, Lerner JM. The blazing of holographic gratings using ion-etching. In: Proc SPIE, Adar F, Griffiths JE, Lerner JM, editors. 1989;1055.
12. Féry C. Comptes Rondue 1910;150:216.
13. Hecht E. Optics. Reading, Massachusetts: Addison-Wesley; 1979.
14. Loewen EG, Popov E. Instrumental Systems. Diffraction Gratings and Applications. New York: Marcel Dekker; 1997. p 437–480.
15. Shapiro H. Practical Flow Cytometry. New York: Wiley-Liss; 1995. p 106–135.
16. Murty MVRK. Compensation for coma and anamorphic effect in double monochromators. Appl Opt 1972;11:1637–1638.
17. Reader J. Optimizing Czerny-Turner spectrographs: A comparison between analytical theory and ray tracing. J Opt Soc Am 1969; 59: 1189–1196.
18. Beutler HG. The theory of the concave grating. J Opt Soc Am 1945; 35:311–350.
19. Chrisp M. Aberration corrected holographic gratings and their mountings. In: Wyant J, Shannon RR, editors. Applied Optics and Optical Engineering, Vol. X. SPIE; 1987. p 391–454.
20. Pieuchard G, Flamand J, Passereau G. Monochromator with concave grating. US Pat. 3,930,728, 1976.
21. Balaban RS, Kurtz I, Cascio HE, Smith PD. Microscopic spectral imaging using a video camera. J Microsc 1986;141:31–34.
22. Benedetti PA, Evangelista V, Guidarini D, Vestri S. Confocal-line microscopy. J Microsc 1992;165:119–129.
23. Warren DW, Hackwell JA. Compact prism spectrograph suitable for broadband spectral surveys with array detectors. US Pat. 5,127,728, 1992.
24. Warren DW, Hackwell JA, Gutierrez DJ. Compact prism spectrographs based on aplanatic principles. Opt Eng 1997;36:1174–1182.
25. National Institute of Standards and Technology (NIST). Atomic Spectra Database: Lines Data. NIST, 2000.
26. Lerner JM, Zucker RM. Calibration and validation of confocal spectral imaging systems. Cytometry A 2004;62:8–34.
27. Centonze V, Pawley J. Tutorial on practical confocal microscopy and use of the confocal test specimen. In: Pawley J, editor. Handbook of Biological Confocal Microscopy, 2nd edition. New York: Plenum; 1995. p 559–567.
28. Centonze V, Pawley J. Practical laser scanning confocal light microscopy: Obtaining optimum performance from your instrument. In: Celis J, editor. Cell Biology, 2nd edition. New York: Academic Press; 1998. Vol. 3, p 149–169.
29. Pawley J. Fundamental limits in confocal microscopy. In: Pawley J, editor. Handbook of Biological Confocal Microscopy. New York: Plenum; 1995. p 19–36.
30. Wilson T. The role of the pinhole in confocal imaging systems. In: Pawley J, editor. Handbook of Biological Confocal Microscopy, 2nd edition. New York: Plenum; 1995. p 167–182.